Table 2 Multiparameter analysis of affected siblings

Patient	Age (years)	Ly (mm^3)	Plt ($\times 10^3/mm^3$)	AFP (ng/mL)	T-chol (mg/dL)	TG (mg/dL)	IgG (mg/dL)	IgM (mg/dL)	IgA (mg/dL)	IgE (ng/mL)	Died (age)
Normal range		1,300–5,300	100–400	<10	150–220	50–150	800–1,600	50–280	100–400	0–380	
1 EB	8.3	3,280	323	n.t.	n.t.	n.t.	**220**	**436**	**0**	n.t.	10.5
1 YB	8.0	1,740	395	135	147	n.t.	**1,000**	**150**	**238**	68	15.0
2 ES	20.0	2,130	380	525	187	n.t.	1,464	360	140	280	20.0
2 YS	9.6	3,240	n.t.	690	160	n.t.	1,008	215	328	68	20[b]
3 EB	11.9	**4,060**	334	**1,090**	177	n.t.	1,130	224	0.8	0	20.4
3 YB	7.5	**1,185**	n.t.	**273**	n.t.	n.t.	1,240	274	0.8	0	14[b]
4 ES	13.7	1,950	329	529	223	n.t.	1,502	239	**30**	n.t.	15.0
4 YS[a]	19.2	1,590	417	524	164	100	1,860	278	**749**	<1	28.2
5 TwB	27.3	1,530	426	n.t.	186	n.t.	n.t.	n.t.	n.t.	n.t.	28.6 (A)
5 TwB	27.3	2,060	492	n.t.	n.t.	n.t.	n.t.	n.t.	n.t.	n.t.	28.6 (A)
6 EB	16.8	1,260	423	316	n.t.	n.t.	1,950	266	**163**	7 IU/mL	22.6 (A)
6 YB	10.8	1,130	504	n.t.	n.t.	n.t.	1,690	256	**2**	<4 IU/mL	16.6[b]
7 ES[a]	11.7	1,250	620	**949**	167	195	852	257	**369**	<1	12.8 (A)
7 YB[a]	5.2	1,180	422	**226**	209	67	1,095	300	**24**	<1	6.3 (A)
8 ES	24.0	1,780	465	**420**	n.t.	n.t.	700	250	179	n.t.	19.0
8 YB	19.0	1,300	n.t.	**1,518**	n.t.	n.t.	755	122	213	<2.0	26.5 (A)
9 EB[a]	19.6	1,320	324	838	177	100	1,144	104	111	14	21.0 (A)
9 YB[a]	17.2	1,500	533	632	144	150	793	89	329	0.9	18.6 (A)
10 ES	11.8	700	429	560	186	66	1,120	224	128	n.t.	28.1
10 YS	9.8	690	490	560	209	121	1,150	168	80	n.t.	31.7
11 ES	4.0	**2,280**	212	100	143	95	**1,703**	**190**	64	<30	5.8
11 YS[a]	3.4	**460**	149	93	125	104	**136**	**3,932**	75	<1	4.0 (A)
12 EB[a]	10.6	**4,820**	**75**	296	117	**499**	**50**	**4,000**	**10**	1	11.6 (A)
12 YB[a]	8.9	**1,070**	**251**	357	133	**22**	**1,070**	**191**	**346**	3	9.7 (A)
13 ES	24.4	730	**454**	**292**	175	88	<5	**790**	<5	<5	24.7
13 YS[a]	22.9	1,250	**374**	**1,662**	197	97	**991**	**263**	**191**	n.t.	23.0 (A)

Ly lymphocytes, *TG* triglyceride, *EB* elder brother, *ES* elder sister, *YB* younger brother, *YS* younger sister, *TwB* twin brother, *n.t.* not tested, *A* alive

[a] Mutation in ATM gene was confirmed

[b] The age of the patient at his/her last visit. Bold indicates data where difference among siblings was noted

his brother was 2.1/4.4%. Decrease in the memory B cell fraction was noted in another patient with HIGM (0.9/10.9%). Unfortunately, lymphocyte immunophenotyping of the patient's elder sister could not be recorded because of her early death from leukemia.

4 Discussion

Toxicity of antineoplastic agents was highlighted as an important issue for treating malignancy in AT patients. Two patients in our cohort developed left cardiac failure after an anthracycline-containing therapeutic regimen. Hemorrhagic cystitis was observed in 2 patients. Anecdotal reports suggest that telangiectasia can occur in the bladder wall; however, symptoms resulting from telangiectasia have only been recently reported in one case who had a history of nephritis and ITP [27, 29]. Our data show that this was not because of peculiarity of the reported patient. The cystitis was most likely related to late toxicity of cyclophosphamide. Although hemorrhagic cystitis is the common adverse effect of high-dose cyclophosphamide, it occurs in less than 5% of patients receiving the conventional dose. Severe cyclophosphamide-related cystitis that requires surgical intervention is rare. Hematuria might begin immediately or occur several years following treatment [30–32]. Therefore, the physicians should be aware of the late side effects of cyclophosphamide administered to AT patients.

Half of the AT patients developing malignancy died of infection or therapy-related toxicity, while 7 of 10 AT patients developed lymphoid malignancy after the age of

9 years, 2 developed B cell malignancy before the age of 6 years (at 4 and 5.7), when diagnosis of AT was not yet established. Both patients died of therapy-related toxicity. To improve early diagnosis of AT, routine measurement of AFP is strongly recommended on diagnosis of B cell malignancy in ataxic children. This would help in finding AT patients who have developed ALL and would require dose modification upon the treatment. Supervision by an oncologist familiar with the specific problems encountered by AT patients would also be beneficial for treatment of malignancy in AT patients.

Severe viral infection has not been a hallmark of AT children in previous surveys, despite their defective antibody response and impaired cellular immunity [8]. Of the 11 patients with severe viral infections, 7 had infections caused by herpesvirus species (3 EBV, 2 VZV, 1 CMV, and 1 HSV). Reduced $CD3^{+}$T cell counts with the absence of lymphopenia or hypogammaglobulinemia were noted in 5 patients, suggesting that those with T-lymphopenia are susceptible to herpesvirus infection.

It is of interest that 5 AT patients showed abnormal anti-EBV titers indicative of persistently active EBV infection, among whom 3 patients also displayed clinical symptoms of EBV infection. Further prospective large-scale study is warranted to investigate immunity against the herpesvirus species in AT children [33].

HIGM phenotype indicative of defective class switch recombination (CSR) has been documented in AT patients; however, it is considered to be infrequent, and its incidence was hitherto unknown. ATM protein is involved in CSR [34–38]. The CSR junctions in B cells from AT patients show a dependence on microhomologies and are devoid of normally occurring mutations around the breakpoint. In our study, AT patients showed deficiencies of serum IgA (in 60% of the patients), IgE (in 80%), IgG (in 26%), and IgG2 (in 80%).

In a previous study, 8% of AT patients developed dysgammaglobulinemia with gammopathy. In our study, 8 patients (16%) showed decreased serum IgG and IgA/E levels. Panhypogammaglobulinemia was documented in 3 patients. It should be noted that 2 of 3 patients with panhypogammaglobulinemia developed lymphoid malignancy. Five patients in our study (10%) showed the HIGM phenotype, and 3 of them showed markedly elevated serum IgM with low IgG level (<200 mg/dL). In fact, 1 patient was initially diagnosed with female HIGM syndrome with mild ataxia. Recent study has shown the immunological phenotype could be reminiscent of hyper-IgM syndrome in patients with AT [27, 39], and our study has shown the hyper-IgM phenotype is not rare in the patients.

Further immunological data were available for 4 of 5 AT patients with HIGM. Some aspects of their data are informative for considering possible mechanisms of the CSR defect. First, HIGM was observed at early childhood before development of bacterial/viral infection. Second, 4 AT patients with HIGM had siblings with AT, and they showed normal IgG/M levels. Third, TRECs in 2 HIGM-AT patients were especially low with <100 TRECs/μgDNA. These data indicate that the HIGM phenotype was not determined solely by ATM mutation type or by the expression level of ATM protein, but possibly by overall recombination activity with other modifier genes or with environmental factors other than infections. Moreover, 12 sibling pairs showed substantially different IgA levels. More detailed analysis of AT children with hypogammaglobulinemia will lead to better understanding of the involvement of ATM in V(D)J recombination and in CSR.

Finally, we evaluated whether the phenotypic variations were due to the mutation type or the age difference by comparing the phenotypes and laboratory data between the sibling pairs with the same ATM mutations. The data were accumulated at a similar age whenever possible.

Our study demonstrated some similarity and difference in the clinical phenotypes and a wide variety in the immunological parameters of the sibling pairs. Thus, it is not likely that the variations were due to age difference or ATM mutation type. The diverse phenotypes and immunological data of the sibling cases suggest a modifier gene(s) and environmental factor(s), or both also serve as important determinants of the patients' phenotypes.

Our data demonstrate that median age at diagnosis, onset of telangiectasia, and longevity were similar to those of previous reports [4, 5, 7]. The most common cause of death was infection, particularly lower respiratory infection at older ages. The proportion of AT patients who developed chorea, malignancy, diabetes mellitus, or short stature was not different from data previously reported.

This paper described the results of the first nationwide survey of AT patients in Japan. Despite the limitations associated with a retrospective study, our data shed light on important issues in AT patients. These data will lead to better patient care as well as understanding of pathogenesis and diverse phenotypes of AT children.

Acknowledgments This work was in part supported by grants from the Ministry of Health, Labour, and Welfare and from the Ministry of Education, Culture, Sports, Science, and Technology to SM and TM.

Conflict of interest statement We have no financial relationships or conflict of interest relevant to this manuscript to be disclosed.

References

1. Claret Teruel G, Giner Munoz MT, Plaza Martin AM, Martin Mateos MA, Piquer Gibert M, Sierra Martinez JI. Variability of immunodeficiency associated with ataxia telangiectasia and

clinical evolution in 12 affected patients. Pediatr Allergy Immunol. 2005;16:615–8.
2. Gatti RA. Ataxia-telangiectasia. In: Scriver CR, Beaudet AL, Sly WS, editors. Metabolic and molecular basis of inherited diseases. New York: Mcgraw-Hill; 2001. p. 1187–96.
3. Gatti RA, Becker-Catania S, Chun HH, Sun X, Mitui M, Lai CH, et al. The pathogenesis of ataxia-telangiectasia. Learning from a Rosetta Stone. Clin Rev Allergy Immunol. 2001;20:87–108.
4. Perlman S, Becker-Catania S, Gatti RA. Ataxia-telangiectasia: diagnosis and treatment. Semin Pediatr Neurol. 2003;10:173–82.
5. Cabana MD, Crawford TO, Winkelstein JA, Christensen JR, Lederman HM. Consequences of the delayed diagnosis of ataxia-telangiectasia. Pediatrics. 1998;102:98–100.
6. Moin M, Aghamohammadi A, Kouhi A, Tavassoli S, Rezaei N, Ghaffari SR, et al. Ataxia-telangiectasia in Iran: clinical and laboratory features of 104 patients. Pediatr Neurol. 2007;37:21–8.
7. Crawford TO, Skolasky RL, Fernandez R, Rosquist KJ, Lederman HM. Survival probability in ataxia telangiectasia. Arch Dis Child. 2006;91:610–1.
8. Nowak-Wegrzyn A, Crawford TO, Winkelstein JA, Carson KA, Lederman HM. Immunodeficiency and infections in ataxia-telangiectasia. J Pediatr. 2004;144:505–11.
9. Vacchio MS, Olaru A, Livak F, Hodes RJ. ATM deficiency impairs thymocyte maturation because of defective resolution of T cell receptor alpha locus coding end breaks. Proc Natl Acad Sci USA. 2007;104:6323–8.
10. Savitsky K, Bar-Shira A, Gilad S, Rotman G, Ziv Y, Vanagaite L, et al. A single ataxia telangiectasia gene with a product similar to PI-3 kinase. Science. 1995;268:1749–53.
11. Lange E, Borresen AL, Chen X, Chessa L, Chiplunkar S, Concannon P, et al. Localization of an ataxia-telangiectasia gene to an approximately 500-kb interval on chromosome 11q23.1: linkage analysis of 176 families by an international consortium. Am J Hum Genet. 1995;57:112–9.
12. Taylor AM, Byrd PJ. Molecular pathology of ataxia telangiectasia. J Clin Pathol. 2005;58:1009–15.
13. Shiloh Y. ATM and related protein kinases: safeguarding genome integrity. Nat Rev Cancer. 2003;3:155–68.
14. Shiloh Y. The ATM-mediated DNA-damage response: taking shape. Trends Biochem Sci. 2006;31:402–10.
15. Reliene R, Schiestl RH. Antioxidants suppress lymphoma and increase longevity in ATM-deficient mice. J Nutr. 2007;137:229S–32S.
16. Reliene R, Schiestl RH. Antioxidant *N*-acetyl cysteine reduces incidence and multiplicity of lymphoma in Atm deficient mice. DNA Repair (Amst). 2006;5:852–9.
17. Du L, Pollard JM, Gatti RA. Correction of prototypic ATM splicing mutations and aberrant ATM function with antisense morpholino oligonucleotides. Proc Natl Acad Sci USA. 2007;104:6007–12.
18. Lai CH, Chun HH, Nahas SA, Mitui M, Gamo KM, Du L, et al. Correction of ATM gene function by aminoglycoside-induced read-through of premature termination codons. Proc Natl Acad Sci USA. 2004;101:15676–81.
19. Oguchi K, Takagi M, Tsuchida R, Taya Y, Ito E, Isoyama K, et al. Missense mutation and defective function of ATM in a childhood acute leukemia patient with MLL gene rearrangement. Blood. 2003;101:3622–7.
20. Takagi M, Tsuchida R, Oguchi K, Shigeta T, Nakada S, Shimizu K, et al. Identification and characterization of polymorphic variations of the ataxia telangiectasia mutated (ATM) gene in childhood Hodgkin disease. Blood. 2004;103:283–90.
21. Gilad S, Chessa L, Khosravi R, Russell P, Galanty Y, Piane M, et al. Genotype-phenotype relationships in ataxia-telangiectasia and variants. Am J Hum Genet. 1998;62:551–61.
22. Birrell GW, Kneebone K, Nefedov M, Nefedova E, Jartsev MN, Mitsui M, et al. ATM mutations, haplotype analysis, and immunological status of Russian patients with ataxia telangiectasia. Hum Mutat. 2005;25:593.
23. Morio T, Hanissian S, Geha RS. Characterization of a 23-kDa protein associated with CD40. Proc Natl Acad Sci USA. 1995;92:11633–6.
24. Morio T, Hanissian SH, Bacharier LB, Teraoka H, Nonoyama S, Seki M, et al. Ku in the cytoplasm associates with CD40 in human B cells and translocates into the nucleus following incubation with IL-4 and anti-CD40 mAb. Immunity. 1999;11:339–48.
25. Morio T, Nagasawa M, Nonoyama S, Okawa H, Yata J. Phenotypic profile and functions of T cell receptor-gamma delta-bearing cells from patients with primary immunodeficiency syndrome. J Immunol. 1990;144:1270–5.
26. Al-Harthi L, Marchetti G, Steffens CM, Poulin J, Sekaly R, Landay A. Detection of T cell receptor circles (TRECs) as biomarkers for de novo T cell synthesis using a quantitative polymerase chain reaction-enzyme linked immunosorbent assay (PCR-ELISA). J Immunol Methods. 2000;237:187–97.
27. Suzuki K, Tsugawa K, Oki E, Morio T, Ito E, Tanaka H, et al. Vesical varices and telangiectasias in a patient with ataxia telangiectasia. Pediatric Nephrology. 2008;23:1005–8.
28. Giovannetti A, Mazzetta F, Caprini E, Aiuti A, Marziali M, Pierdominici M, et al. Skewed T-cell receptor repertoire, decreased thymic output, and predominance of terminally differentiated T cells in ataxia telangiectasia. Blood. 2002;100:4082–9.
29. Chun HH, Gatti RA. Ataxia-telangiectasia, an evolving phenotype. DNA Repair (Amst). 2004;3:1187–96.
30. Marshall FF, Klinefelter HF. Late hemorrhagic cystitis following low-dose cyclophosphamide therapy. Urology. 1979;14:573–5.
31. Stillwell TJ, Benson RC Jr. Cyclophosphamide-induced hemorrhagic cystitis. A review of 100 patients. Cancer. 1988;61:451–7.
32. Walker RD. Cyclophosphamide induced hemorrhagic cystitis. J Urol. 1999;161:1747.
33. Mizutani S. Genetic background as a possible determinant of clinical and biological features of Epstein-Barr virus infection—a hypothetical view. Crit Rev Oncol Hematol. 2002;44:217–25.
34. Pan Q, Petit-Frere C, Lahdesmaki A, Gregorek H, Chrzanowska KH, Hammarstrom L. Alternative end joining during switch recombination in patients with ataxia-telangiectasia. Eur J Immunol. 2002;32:1300–8.
35. Pan-Hammarstrom Q, Dai S, Zhao Y, van Dijk-Hard IF, Gatti RA, Borresen-Dale AL, et al. ATM is not required in somatic hypermutation of VH, but is involved in the introduction of mutations in the switch mu region. J Immunol. 2003;170:3707–16.
36. Pan-Hammarstrom Q, Lahdesmaki A, Zhao Y, Du L, Zhao Z, Wen S, et al. Disparate roles of ATR and ATM in immunoglobulin class switch recombination and somatic hypermutation. J Exp Med. 2006;203:99–110.
37. Peron S, Pan-Hammarstrom Q, Imai K, Du L, Taubenheim N, Sanal O, et al. A primary immunodeficiency characterized by defective immunoglobulin class switch recombination and impaired DNA repair. J Exp Med. 2007;204:1207–16.
38. Reina-San-Martin B, Chen J, Nussenzweig A, Nussenzweig MC. Enhanced intra-switch region recombination during immunoglobulin class switch recombination in 53BP1−/− B cells. Eur J Immunol. 2007;37:235–9.
39. Soresina A, Meini A, Lougaris V, Cattaneo G, Pellegrino S, Piane M, et al. Different clinical and immunological presentation of ataxia-telangiectasia within the same family. Neuropediatrics. 2008;39:43–5.

Immunologically silent cancer clone transmission from mother to offspring

Takeshi Isoda[a,1], Anthony M. Ford[b,1], Daisuke Tomizawa[a], Frederik W. van Delft[b], David Gonzalez De Castro[b], Norkio Mitsuiki[a], Joannah Score[c], Tomohiko Taki[d], Tomohiro Morio[a], Masatoshi Takagi[a], Hiroh Saji[e], Mel Greaves[b,2,3], and Shuki Mizutani[a,2,3]

[a]Department of Pediatrics and Developmental Biology, Tokyo Medical and Dental University, 1-5-45 Yushima, Bunkyo-ku, Tokyo 1138519, Japan; [b]Section of Haemato-Oncology, Institute of Cancer Research, Brookes Lawley Building, 15 Cotswold Road, Sutton, Surrey SM2 5NG, United Kingdom; [c]Wessex Regional Genetics Laboratory, University of Southampton, Salisbury District Hospital, Salisbury SP2 8BJ, United Kingdom; [d]Department of Molecular Laboratory Medicine, Kyoto Prefectural University of Medicine Graduate School of Medical Science, 465 Kajii Cho, Hirokoji-agaru, Kawaramachi, Kamigyo-ku, Kyoto 6028566, Japan; and [e]Human Leukocyte Antigen Laboratory, Ebis Building, 3-4F, 82 Shimo-Tsutsumimachi, Marutamachi-kudaru, Kawabata Dori, Sakyo-ku, Kyoto 606-8396, Japan

Edited by Janet D. Rowley, University of Chicago Medical Center, Chicago, IL, and approved July 28, 2009 (received for review April 28, 2009)

Rare cases of possible materno-fetal transmission of cancer have been recorded over the past 100 years but evidence for a shared cancer clone has been very limited. We provide genetic evidence for mother to offspring transmission, in utero, of a leukemic cell clone. Maternal and infant cancer clones shared the same unique *BCR-ABL1* genomic fusion sequence, indicating a shared, single-cell origin. Microsatellite markers in the infant cancer were all of maternal origin. Additionally, the infant, maternally-derived cancer cells had a major deletion on one copy of chromosome 6p that included deletion of HLA alleles that were not inherited by the infant (i.e., foreign to the infant), suggesting a possible mechanism for immune evasion.

fetus | fusion gene | leukemia

Rare cases of melanoma or hemopoietic malignancies in infants have been recorded that may have been of maternal origin (1). Genetic evidence for a shared, materno-fetal clone of cancer cells has, however, to date, been sparse and based upon limited karotype information (1). Unambiguous attribution of transmission of a cancer clone should be achievable by genetic fingerprinting, the most striking precedent for which is canine transmissible venereal sarcoma (CTVS) in which multiple cases worldwide derive from a single clone (2). Leukemia fusion genes, generated by chromosome translocations, have patient-specific or idiosyncratic genomic sequences at the fusion breakpoints and are frequently early or initiating events (3). They therefore provide stable, specific, and sensitive clonal markers and can unambiguously identify a single-cell origin in different individuals as documented with monozygotic twins with concordant leukemia (4). We report here equivalent genetic scrutiny of a case of concordant maternal and infant ALL/lymphoma with the *BCR-ABL1* fusion gene.

Results

The Mother. The Japanese mother was 28 years old at her child's delivery. No hematological abnormalities had been identified during the pregnancy, and the birth was uncomplicated. Thirty-six days after the delivery, the mother experienced vaginal bleeding. On day 39, she developed fever, and on day 43, bleeding became uncontrollable. Blood showed leukocytosis (206,800/μL) with 97% lymphoblasts, anemia (hemoglobin level: 3.5g/dL), and thrombocytopenia (platelet count: $0.2 \times 10^4/\mu$L). Bone marrow aspiration revealed peroxidase-negative lymphoblasts (99.6% of nucleated cells), which were positive for CD10, CD19, CD20, CD34, TdT, and CD79a. Chromosomal G-banding showed 46,XX,t (9, 22)(q34;q11), and 3.2×10^5 copies/μgRNA of p190-type *BCR-ABL1* mRNA were detected by RT-PCR. She was diagnosed as having B-cell precursor Ph+ ALL (see *SI Text* for clinical treatment).

The Infant. The 11-month-old female offspring of the above mother was admitted to hospital with right cheek swelling. MRI revealed a mass in the cheek (Fig. S1*A*) and a pleural effusion of the lung. There was no lymph node swelling or organomegaly. She was born with normal delivery at 40 weeks, 5 days gestation. There was no history of prenatal abnormalities including intrauterine growth retardation, and she showed normal growth and development until admission.

Laboratory Findings on Infant Samples. Laboratory analyses of the maternal and infant samples was carried out with full ethical approval in accordance with the Declaration of Helsinki (Local ethics approval # CCR2285) and with informed consent of the family (father). Biopsy of the primary jaw tumor showed the presence of small round blue cell tumor with large nucleus/cytoplasm ratio, which diffusely proliferated with partial hyalinization of stroma. A large antibody panel was used to distinguish a sarcoma from lymphoma. LCA, CD10, CD20, CD79a, TdT, CD34, and MIC2 were positive by immunohistochemical staining, and CD3, CD5, CD56, desmin, HHF35, S100, GFAP, chromogranin, and synaptophysin were all negative. No cytogenetic analysis was performed but subsequent FISH analysis revealed positivity for the *BCR-ABL1* gene (Fig. S1*B*).

Cells (48.2%) in the pleural fluid were positive for CD10, CD19, CD34, and HLA-DR and p190-type *BCR-ABL1* chimeric mRNA was detected (9.5×10^4 copies/μgRNA) by quantitative RT-PCR (Q-PCR).

Blood count findings on the infant were as follows; WBC 10,100/μL (segment forms 22%; lymphocytes 72%; monocytes 5%; eosinophil 1%), hemoglobin level 12.5 g/dL, platelet count $38.4 \times 10^4/\mu$L. No blast cells were detected in the cerebrospinal fluid, and there was no morphological evidence of tumor infiltration in bone marrow. Bone marrow aspirates were negative for *BCR-ABL1* chimeric mRNA by Q-PCR. The patient's neoplastic cells had the same immunophenotype and abnormal genotype (*BCR-ABL1* fusion) as her mother's ALL but, in light of the presentation features, she was diagnosed as having B-cell precursor lymphoblastic lymphoma stage III by the St. Jude Staging System (see *SI Text* for clinical treatment of infant).

Author contributions: M.G. and S.M. designed research; A.M.F., D.T., F.W.v.D., D.G.D.C., N.M., J.S., T.T., T.M., M.T., and H.S. performed research; T.I. contributed new reagents/analytic tools; M.G. and S.M. analyzed data; and M.G. and S.M. wrote the paper.

The authors declare no conflict of interest.

This article is a PNAS Direct Submission.

[1]T.I. and A.M.F. contributed equally to this work.

[2]M.G. and S.M. contributed equally to this work.

[3]To whom correspondence may be addressed. E-mail: mel.greaves@icr.ac.uk or skkm12@gmail.com.

This article contains supporting information online at www.pnas.org/cgi/content/full/0904658106/DCSupplemental.

www.pnas.org/cgi/doi/10.1073/pnas.0904658106

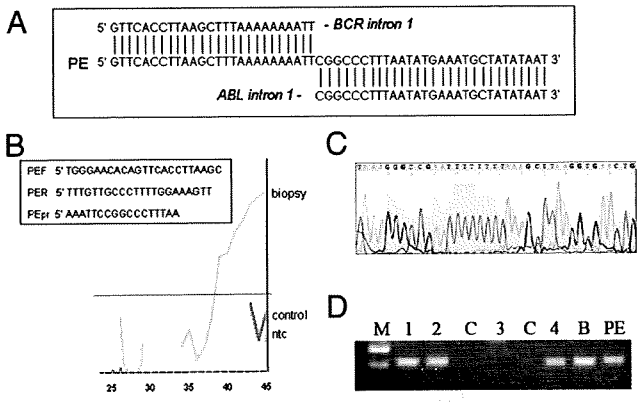

Fig. 1. Characterization of the *BCR-ABL1* fusion gene. (*A*) Comparison of the pleural effusion (PE) *BCR-ABL1* breakpoint DNA sequence with *BCR* intron 1 (NM_004327) and *ABL1* intron 1 (NM_007313) sequences. (*B*) Q-PCR amplification of the *BCR-ABL1* breakpoint in WGA DNA from mother's bone marrow biopsy. The primers and probe shown were chosen to span the PE fusion sequence obtained from the child's PE DNA. (*C*) Reverse strand DNA sequence of DNA from the mother's biopsy showing the same *BCR-ABL1* fusion sequence as found in the child. (*D*) PCR of the *BCR-ABL1* breakpoint in DNA from the neonatal blood spot confirming presence of the *BCR-ABL1* fusion gene. Lanes 1–4: slices from the child's card (1, 2, and 4 positive), C: DNA from control neonatal blood spot, B: mother's marrow biopsy DNA. PE: child's pleural effusion DNA. M: marker.

***BCR-ABL1* Genomic Fusion Sequencing.** We first cloned the *BCR-ABL1* genomic breakpoint region from the infant's pleural effusion (PE) (see *Materials and Methods*). DNA was Whole Genome Amplified (GenomiPhi, GE Healthcare), according to the manufacturer's instructions. The breakpoint was designated as a fusion between *BCR* intron 1 (46110 bp from ATG: NM_004327) and *ABL1* intron 1 (118930 bp from ATG: NM_007313) (Fig. 1*C*).

DNA from the mother's bone marrow was isolated by scraping cells from a formalin fixed paraffin embedded (FFPE) biopsy slide (the only sample available) using Recoverall (Ambion) as suggested by the manufacturer. Fragmented FFPE DNA was then subjected to whole genome amplification (WGA), and 2 μL amplified DNA subjected to 45 cycles Q-PCR with primers designed by Primer 3 software (5) and described in Fig. 1*B* and a FAM-labeled probe that spanned the specific *BCR-ABL1* breakpoint sequence. After successful Q-PCR (Fig. 1*B*), the product was purified and sequenced using the reverse *ABL1* primer. The fusion sequence in the mother's biopsy was verified as identical to that obtained from the pleural effusion of the child (Fig. 1*C*).

The archived neonatal blood spot (Guthrie card) of the infant was screened for the clonotypic *BCR-ABL1* genomic sequence using specific primers and as previously described for other fusion genes (6). Three out of four blood spot slices were positive (Fig. 1*D*), indicating that the cancer clone was present in the blood at birth.

Microsatellite Markers. Short tandem repeat (STR) microsatellite analysis of the DNA extracted from the jaw biopsy showed one predominant population (>95% of alleles) that did not correspond to the DNA profile obtained from the paternal sample (Fig. 2). The STR profile shows that it shared one allele with the patient's germline DNA for all of the 15 STR markers studied which was different from the paternally-inherited alleles, demonstrating that the jaw tumor sample was of maternal origin

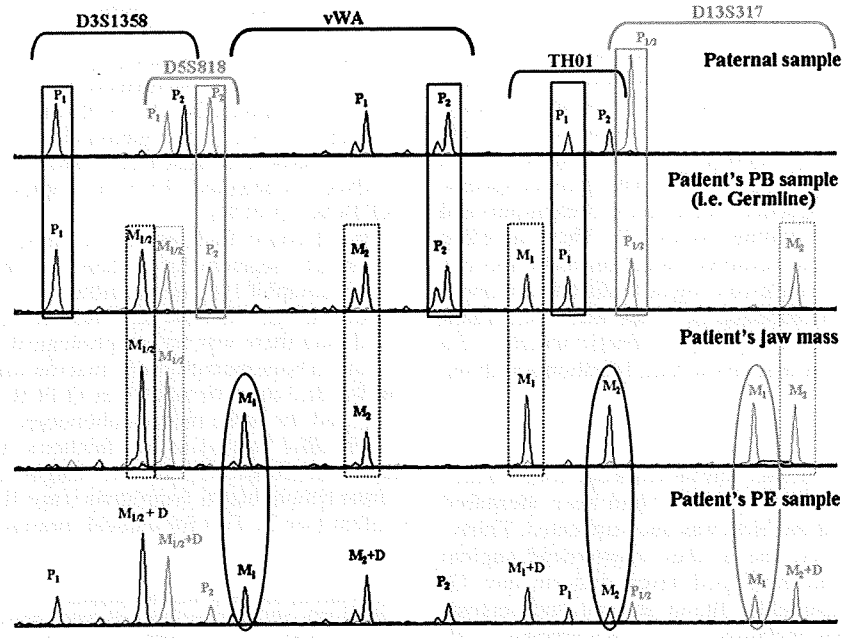

Fig. 2. STR typing for the paternal sample and patient's peripheral blood (PB), lymphoma (from the jaw mass) and pleural effusion samples. Figure shows typing for five out of the 15 STR markers analyzed. The STR profile of patient's jaw mass shows the sharing of one allele with the patient's germline DNA for all markers while the other allele is not present in the paternal DNA, demonstrating that the lymphoma DNA obtained from the jaw mass contained >95% of maternal cells. For each STR marker the Paternal (P1, P2) and Maternal (M1, M2) alleles are indicated. P and M alleles contributing to the patient's germline DNA are contained within solid and dotted rectangles, respectively. The PE sample shows a mixture of different alleles, with some markers showing up to three different alleles (vWA, TH01, and D13S317, contained in ovals), indicating heterozygosity for the maternal genotype on these markers. The remaining maternal alleles contributing to the daughter's genotype in this sample are indicated as M + D. These former markers were used for calculation of the percentage of maternal cells present in the PE sample (≈50–60%) by comparing the areas of the maternal-only peaks (M) versus the paternal peaks (corresponding to the patient's cells). This proportion of maternal cells approximates with the percentage tumor infiltration identified by immunophenotype (48.2%).

Table 1. Loss of non-inherited maternal HLA allele expression in infants 'maternal' cancer cells

	HLA-A	HLA-B	DRB1
Father	A2/A33	B61/B58	DR8/DR13
Mother	A24/**A11**	B60/**B67**	DR9/**DR15**
Patient	A24/A33 2402/3303	B60/B58 4001/5801	DR9/DR13 0901/1302
Patient's jaw mass	A24/-2402/-	B60/-4001/-	DR9/-0901/-

Alleles were serotyped or genotyped (2402/3303, 4001/5801, 0901/1302) (see *SI Text*). Insufficient material was available to genotype parental samples. Alleles in bold are maternal HLA alleles lost from maternal cancer cells transmitted to infant.

(>95% maternal cells). STR analysis of the PE sample showed a mixture of alleles for most STR markers analyzed. These mixtures were identified either because of the presence of three different alleles in some markers, or because those markers with only two alleles presented an imbalance in the ratio of the peak areas (Fig. 2). These findings were consistent with the presence of two genetically different cell populations in the PE specimen–one maternal, one infant offspring (see Fig. 2 legend).

HLA Analysis. Survival of maternal cells in the offspring presumably requires some form of immunological acceptance or tolerance of cells expressing foreign, non-inherited maternal MHC antigens. We serotyped samples from both parents for HLA-A, HLA-B, and DRB1, and both serotyped and genotyped the infant's normal blood and lymphoma cells. The result was that the *BCR-ABL1*-positive jaw tumor had selectively deleted or lost the HLA alleles that were not inherited by the daughter (Table 1). The nature of this genetic lesion in the infant tumor cancer cells was further explored by high resolution SNP arrays. In the absence of normal germline maternal and infant DNA and only small quantities of degraded DNA from the maternal leukemia biopsy, we elected to analyze the infant lymphoma (jaw) sample for genome-wide lack of heterozygosity (LOH) in comparison with pooled normal control DNA. Table 2 summarizes the LOH analysis of the infant lymphoma. Recurrent deletions of *IKZF1* and *CDKN2A/B* have previously been described in *BCR-ABL1* ALL (7), as have deletions of *EBF1* and *RAG1/2* in B lineage childhood ALL (8). In addition to these anticipated oncogenic or 'driver' deletions, we observed a large region of homozygosity on the short (p) arm of chromosome 6 including the whole HLA locus. This loss was accompanied by duplication of the other parental 6p region resulting in uniparental disomy. A large genomic deletion, including the HLA loci, therefore accounts for the loss of maternal HLA alleles.

Discussion

These data unambiguously mark the infant cancer as of maternal origin. Some 17 cases of probable metastasis to the fetus have now been recorded (1, 9, and current report), the first being in 1866, most being either melanoma (#6), a cancer with a notoriously metastatic proclivity, or leukemia/lymphoma (#8). Given the phenotypic features described in these cases, it is likely that they were all, as presumed, of maternal origin rather than coincidental cancers. Genetic markers can unambiguously resolve cellular origins in this context. In three of the reported leukemia/lymphoma cases, the male infant bone marrow contained cells with an XX karyotype (1). Whilst these most probably do reflect maternal leukemia/lymphoma cells, it cannot be excluded that they were non-malignant, normal maternal cells or infant male cells in which the Y chromosome was lost and X was duplicated. These are, individually, not rare events in leukemia (10, 11), although they seldom occur together in one clone. Other prior evidence for a maternal origin was the identification in a case of NK cell lymphoma of a specific chromosome translocation t(X;1)(q22;q12) in the maternal lymphoma and in three metaphases of the infant tumor (12).

The rarity of materno-fetal transmission of cancer is a testimony to the efficacy of the placental barrier and perhaps to immunosurveillance. In the present case, an additional feature was the selective loss in the infant maternally-derived tumor cells of maternal HLA alleles that were not inherited by the infant (Tables 1 and 2). Loss of HLA would be expected to render the transmitted cancer cells immunologically inert (13). HLA loci encoded cell surface proteins provide the major antigenic targets for allograft recognition and rejection, so it is likely that HLA deletion in this case contributed to successful transmission of the maternal leukemic cells. However, given the large size of the 6p deletion, it is possible that other gene losses could have contributed to the apparent lack of immuno-surveillance. Other unusual situations where cancer cell transmission occurs all appear to involve immunological invisibility (14): inter-monozygotic twin transmission in utero (4), immunosuppressed recipients of cancer-infiltrated donor organs (15), down-regulated MHC antigen expression in venereal sarcoma in dogs (2), and lack of MHC diversity in the Tasmanian devil (*Sarcophilus harrisii*) with transmissible facial tumors (16). In a recent report (17), loss of allorecognition of leukemic cell HLA by T cells, in a transplant context, also occurred by acquired uniparental disomy of chromosome 6p in the leukemic cells, as in the present study. It is possible that materno-feto transfer of cancer cells is more common than is reflected in the frequency of clinically diagnosed cases and that immuno-surveillance is the principal constraint.

Table 2. Loss of heterozygosity analysis of infant tumor lymphoma

Region	LOH	Gene(s)
5p33.3	Loss	*EBF1*
6p25.3–21.1	UPD	*HLA*, and many other genes
7p14.1	Loss	*TCRG*
7p12.2	Loss	*IKZF1*
9p21.3–12	Loss	*MTAP, CDKN2A/B, PAX5*
11p12	Loss	*RAG1/2*
14q11.2	Loss	*TCRA*
14q32.33	Loss	*IGH*
15q22.33	Loss	*SMAD3*
22q11.22	Loss	*IGL*

Loss of heterozygosity analysis of the infant tumor lymphoma in comparison with unpaired control DNA. UPD, uniparental disomy (see *Materials and Methods* for details).

Materials and Methods

Detection and Amplification of *BCR-ABL1* Genomic Breakpoints. For detection and amplification of DNA breakpoints, ranging from 300 bp to 12 kbp the Expand Long Template PCR kit (Roche) with System 2 was used, with an annealing temperature of 64 °C. To cover the *BCR* and *ABL1* regions, within which breakpoints can occur, 21 *BCR* forward primers and 20 *ABL1* reverse primers were used in multiplex, combining each *BCR* forward primer with 4 mixes of 5 *ABL1* reverse primers.

The child's genomic breakpoint was initially amplified using *BCR* 3C F (GGGCTCATTTTCACTGGATGGAC) and the *ABL1* D reverse primer mix, and

upon split out PCR, a band was amplified with *BCR* 3C F and *ABL1* 1D R (AGC CAT AAC CAT TCT CCC AAG CA). The breakpoint was confirmed by re-amplification and sequencing of the breakpoint in both the original and WGA amplified patient sample with *BCR* 3C F (GGGCTCATTTTCACTGGATGGAC), and a breakpoint specific *ABL1* reverse primer (TTC AGG GGC CTT GGA TCA GAC TA) determined from sequencing the original cloned product. Forward and reverse primers for blood spot PCR were respectively (GATCCTTTTAAAT-AGGCAAG) and (GTAATGCCAAAAATAACACT).

Fifteen polymorphic STR markers were amplified in the paternal blood DNA and patient's PE and PB DNA samples using the Powerplex-16 system (Promega).

Genome Mapping Analysis. Mapping analysis was performed using 500 ng of tumor DNA from the infant lymphoma. DNA was prepared according to manufacturer's instructions using the GeneChip mapping 500K assay protocol for hybridization to GeneChip Mapping 250K Nsp and Sty arrays (Affymetrix). Briefly, genomic DNA was digested in parallel with restriction endonucleases *Nsp*I and StyI, ligated to an adaptor, and subjected to PCR amplification with adaptor-specific primers. The PCR products were digested with *DNase*I and labeled with a biotinylated nucleotide analog. The labeled DNA fragments were hybridized to the microarray, stained by streptavidin–phycoerythrin conjugates, and washed using the Affymetrix Fluidics Station 450 then scanned with a GeneChip scanner 3000 7G.

Copy Number and LOH Analysis. SNP genotypes were obtained using Affymetrix GCOS software (version 1.4) to obtain raw feature intensity and Affymetrix GTYPE software (version 4.0) using the Dynamic Model algorithm with a call threshold of 0.33 to derive SNP genotypes. The sample was analyzed using CNAG 3.0 (http://plaza.umin.ac.jp/genome), comparing tumor sample with unpaired control DNA to determine copy number and LOH caused by imbalance (18).

HLA Typing. Serotyping was by microdroplet lymphocyte cytotoxicity (19). Genotyping was carried out using a reversed SSO HLA DNA typing method using fluorescent microspheres and a flow analyzer (20).

ACKNOWLEDGMENTS. We thank Dr Masafumi Taniwaki and Mr Nakaba Ochiai for support of this work. This research was funded by a Grant-in-Aid of Ministry of Education, Science, Sports, and Culture and Ministry of Health, Labor, and Welfare, Japan (to S.M.) and Leukaemia Research U.K. (to M.G.).

1. Alexander A, et al. (2003) Metastatic melanoma in pregnancy: Risk of transplacental metastases in the infant. *J Clin Oncol* 21:2179–2186.
2. Murgia C, Pritchard JK, Kim SY, Fassati A, Weiss RA (2006) Clonal origin and evolution of a transmissible cancer. *Cell* 126:477–487.
3. Greaves MF, Wiemels J (2003) Origins of chromosome translocations in childhood leukaemia. *Nat Rev Cancer* 3:639–649.
4. Greaves MF, Maia AT, Wiemels JL, Ford AM (2003) Leukemia in twins: Lessons in natural history. *Blood* 102:2321–2333.
5. Rozen S, Skaletsky HJ (2000) Primer3 on the WWW for general users and for biologist programmers. *Bioinformatics Methods and Protocols: Methods in Molecular Biology*, eds Krawetz S, Misener S (Humana Press, Totowa, NJ), pp 365–386.
6. Gale KB, et al. (1997) Backtracking leukemia to birth: Identification of clonotypic gene fusion sequences in neonatal blood spots. *Proc Natl Acad Sci USA* 94:13950–13954.
7. Mullighan CG, et al. (2008) BCR-ABL1 lymphoblastic leukaemia is characterized by the deletion of Ikaros. *Nature* 453:110–114.
8. Mullighan CG, et al. (2007) Genome-wide analysis of genetic alterations in acute lymphoblastic leukaemia. *Nature* 446:758–764.
9. Maruko K, Maeda T, Kamitomo M, Hatae M, Sueyoshi K (2004) Transplacental transmission of maternal B-cell lymphoma. *Am J Obstet Gynecol* 191:380–381.
10. Heinonen K, Mahlamäki E, Riikonen P, Meltoranta RL, Rahiala J, Perkkiö M (1999) Acquired X-chromosome aneuploidy in children with acute lymphoblastic leukemia. *Med Pediatr Oncol* 32:360–365.
11. United Kingdom Cancer Cytogenetics Group (UKCCG) (1992) Loss of the Y chromosome from normal and neoplastic bone marrows. *Genes Chromosomes Cancer* 5:83–88.
12. Catlin EA, et al. (1999) Transplacental transmission of natural-killer-cell lymphoma. *N Engl J Med* 341:85–91.
13. Seliger B (2005) Strategies of tumor immune evasion. *BioDrugs* 19:347–354.
14. Greaves M (2000) *Cancer. The Evolutionary Legacy* (Oxford Univ Press, Oxford).
15. Penn I (1991) Donor transmitted disease: Cancer. *Transpl Proc* 23:2629–2631.
16. Siddle HV, et al. (2007) Transmission of a fatal clonal tumor by biting occurs due to depleted MHC diversity in a threatened carnivorous marsupial. *Proc Natl Acad Sci USA* 104:16221–16226.
17. Vago L, et al. (2009) Loss of mismatched HLA in leukemia after stem-cell transplantation. *N Engl J Med* 361:478–488.
18. Nannya Y, et al. (2005) A robust algorithm for copy number detection using high-density oligonucleotide single nucleotide polymorphism genotyping arrays. *Cancer Res* 65:6071–6079.
19. Terasaki PI, Bernoco D, Park MS, Ozturk G, Iwaki Y (1978) Microdroplet testing for HLA-A, -B, -C, and -D antigens. *Am J Clin Pathol* 69:103–120.
20. Saito K, et al. (2002) A new reversed SSO HLA (Class I and II) DNA typing method using fluorescently labeled microspheres and flow analyzer. *Eur J Immunogenet* 29:173.

Two Brothers with Ataxia-Telangiectasia-like Disorder with Lung Adenocarcinoma

Naoki Uchisaka, MD, Naomi Takahashi, Masaki Sato, Akira Kikuchi, MD, Shinji Mochizuki, MD, Kohsuke Imai, MD, PhD, Shigeaki Nonoyama, MD, PhD, Osamu Ohara, PhD, Fumiaki Watanabe, PhD, Shuki Mizutani, MD, PhD, Ryoji Hanada, MD, and Tomohiro Morio, MD, PhD

We report on 2 brothers with ataxia-telangiectasia-like disorder with lung adenocarcinoma. They both had ataxia with cerebellar atrophy and mental retardation. They had the same mutation of the *MRE11* gene, which has not been reported previously (c.727T>C and g.24994G>A). *(J Pediatr 2009;155:435-8)*

Ataxia-telangiectasia-like disorder (ATLD) is a rare disease classified under the name of chromosomal breakage syndrome. It is characterized by the clinical features of progressive cerebellar degeneration, increased levels of spontaneously occurring chromosomal aberrations, and increased sensitivity to ionizing radiation with the absence of ocular telangiectasia and immunodeficiency. In 1999, Stewart et al identified *MRE11* mutations from 4 patients with ATLD.[1] Sixteen patients in 6 families have been reported with ATLD.[1-3] Although chromosomal breakage syndromes, such as ataxia-telangiectasia (A-T) and Nijmegen breakage syndrome (NBS), are well known as disorders that predispose patients to malignancy, there has been no earlier report of a patient with ATLD with malignancy. We report on 2 siblings with ATLD in whom lung adenocarcinoma developed.

Case Report

The affected siblings were born to non-consanguineous parents after healthy pregnancies and deliveries. Their parents had a history of diabetes mellitus and smoking, but there was no family history of malignancy.

The brothers had characteristic clinical features of short stature, pointy nose, small jaw, atrophy of the lower legs, and equinus foot deformities. They had cerebellar ataxia, slurred and explosive speech, and ocular apraxia, but did not show any evidence of involuntary movement such as dystonia or dyskinesia. Ataxic gait was noted when they were 2 years old. The boys had been observed for progressive cerebellar ataxia with atrophy of the cerebellum and mental retardation. The degree of cerebellar ataxia and atrophy was more severe in the elder brother, who became wheelchair bound at 6 years of age.

The patients started to speak at 2 years old. One brother's IQ score was 43, and the other's was 75. There was no history of serious infection or evidence of skin or conjunctival telangiectasia. The elder brother was diagnosed with renal Fanconi syndrome; and a renal biopsy showed vacuolar degeneration of the renal tubules.

In 2007, when they were 15 and 9 years old, stage 4 non-small-cell lung cancer (poorly differentiated lung adenocarcinoma with multiple bone metastases) was diagnosed in both boys.

With a laboratory examination, elevation of serum CA125 levels (956.4U/ml and 1449.8U/ml, respectively) and polycythemia were revealed. Serum alpha fetoprotein and immunoglobulin levels were in the reference range (alpha fetoprotein, 5.60 ng/mL and 3.78ng/mLl; immunoglobulin G, 1205 mg/dL and 947 mg/dL). With cytogenetic analysis performed on PHA-stimulated peripheral blood, an increased number of chromosome aberrations, but no specific or particular chromosome abnormalities, was revealed.

Both of the patients received chemotherapy before the diagnosis was made. The elder brother was treated with docetaxel and carboplatin. A half dose of the chemotherapeutic agents was administered because of gastrointenstinal toxicity. He died 11 months after the diagnosis of lung adenocarcinoma.

The younger brother was initially treated with half dose of a docetaxel and cisplatin regimen, and later with irinotecan because of gastrointenstinal toxicity. He also received radiation therapy to the primary tumor. He died 8 months after the diagnosis. Radiation-induced esophagitis was observed in autopsy samples.

ATM deficiency was found to be unlikely, because of the presence of ATM protein that was demonstrated with Western blot analysis (data not shown). We then examined the

A-T	Ataxia-telangiectasia
ATLD	Ataxia-telangiectasia-like disorder
NBS	Nijmegen breakage syndrome

From the Division of Hematology/Oncology, Saitama Children's Medical Center, Saitama, Japan (N.U., A.K., S. Mochizuki, R.H.); Department of Pediatrics, Tokyo Medical and Dental University, Tokyo, Japan (N.T., M.S., F.W., S. Mizutani; T.M.); Department of Pediatrics, National Defense Medical College, Saitama, Japan (K.I., S.N.); and Kazusa DNA Research Institution, Chiba, Japan (O.O.)

This work was supported in part by grants from the Ministry of Health, Labour, and Welfare of Japan (T.M.) and from the Ministry of Education, Culture, Sports, Science Technology of Japan (S. Mizutani and T.M.). The authors declare no conflicts of interest.

0022-3476/$ - see front matter. 10.1016/j.jpeds.2009.02.037

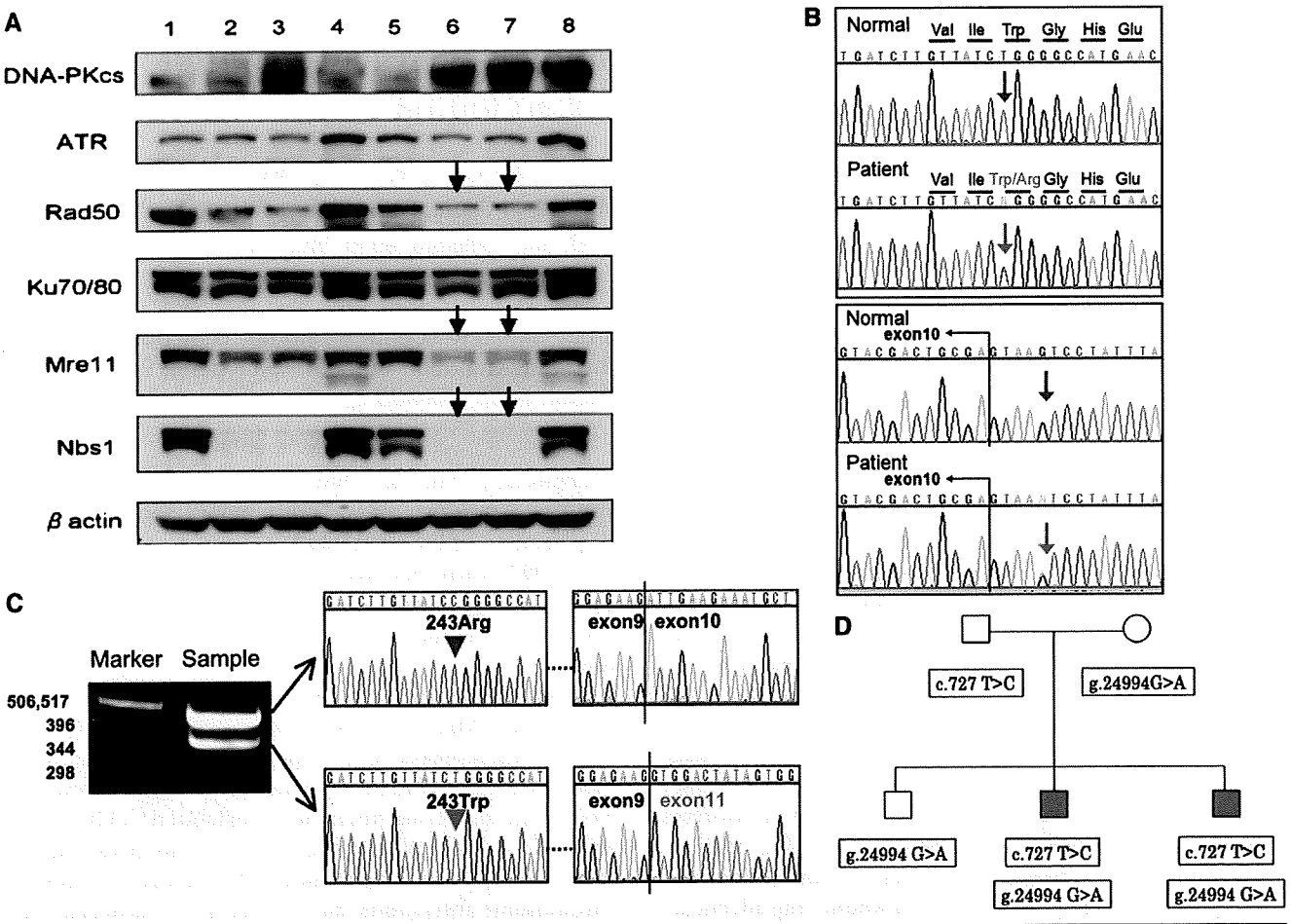

Figure. Mutation analysis of Mre11 deficiency. **A,** Western blot analysis shows alteration in protein levels of Mre11, Nbs1, and Rad50 in the patients. The cell lysates from activated T-cells or EBV-transformed B-cells (EBV-LCL) were subjected to Western blot for detection of indicated proteins. β-actin was included as a control protein to show protein loading in each lane. Lanes 1-4: activated T-cells; Lanes 5-8: EBV-LCL. 1 and 5: healthy control; 2 and 5: elder brother; 3 and 6: younger brother; 4 and 8: A-T patient. **B,** Mutation analysis of *MRE11*. The 20 exons and the flanking intronic regions of *MRE11* gene were sequenced. This revealed c.727 T>C (W243R) in exon 8 and g.24994 G>A in intron 10 that is located 5bp downstream of exon 10, respectively. The sequencing showed T/C in exon 8 and G/A in intron 10; and both mutations are indicated as "N" in the figure. **C,** RT-PCR of exon 7 to exon 11 of *MRE11* cDNA and sequence of the PT-PCR products. Sequencing of 479bp and 398 bp RT-PCR products revealed c. 727 T>C and the deletion of the entire exon 10. **D,** Summary of *MRE11* sequences of the family members.

expression of Mre11, Rad50, and Nbs1 proteins. With the Western blot, severely decreased Nbs1 expression associated with decreased levels of Mre11 and Rad50 was demonstrated in both of the patients (Figure, A). Because we failed to detect *NBS1* gene mutation, we looked for alteration in *MRE11* gene in the 20 exons and the flanking intronic sequences. This revealed a T>C substitution in exon 8 and a base substitution of g.24994 G>A in intron 10, 5bp downstream from exon 10 (Figure, B). RT-PCR of exon 7–exon 11 of *MRE11* complementary DNA of the patients gave us 2 bands (Figure, C). Sequencing of the *MRE11* RT-PCR products revealed a base substitution c.727 T>C in exon 8 in 1 of the alleles and an 81 bp deletion in exon 10 on another allele. The alteration of these DNA sequences predicts an amino acid substitution (W243R) and the loss of 27 amino acids, respectively. The base substitution in intron 10 might have given rise to an alternative splicing of *MRE11*, leading to an in frame 81 bp deletion in exon 10. Thus, the compound heterozygous mutations of *MRE11* gene (c.727 T>C and g.24994 G>A) were identified in both of these brothers (Figure, B and C).

The father was a carrier of c.727 T>C mutation, and the mother and their eldest brother were carriers of g.24994 G>A mutation (Figure, D). The expression level of Mre11 protein was normal in both of these carriers (data not shown).

Discussion

To date, 16 patients have been reported in 6 families with ATLD (Table). Compared with the earlier cases, both of

Table. Clinical features of patients with ataxia-telangiectasia-like disorder

Authors	Year	Nation	Family	Patients	Age at report (years)	Sex	Mutation	Zygosity	Ataxia	Cerebellar atrophy	Occular apraxia	Telangiectasia	Tumors
Stewart et al	1999	Pakistan	1	1	25	F	633R→Stop	Homozygous	+	+		–	–
				2	20	M			+	+		–	–
		England	2	3	18	M	N117S	Compound heterozygous	+	+	+	–	–
				4	15	M	R571X		+	+	+	–	–
Dalia et al	2004	Italy	3	5	37	M	T481K	Compound heterozygous	+	+	+	–	–
				6	36	F	R571X		+	+	+	–	–
Fernet et al	2005	Saudia Arabia	4	7	37	F	W210C	Homozygous	+	+	+	–	–
				8	33	F			+	+	+	–	–
				9	20	M			+	+	+	–	–
				10	20	M			+	+	+	–	–
			5	11	11	F	W210C	Homozygous	+	+	+	–	–
				12	8	F			+	+	+	–	–
				13	7	F			+	+	+	–	–
			6	14	15	F	W210C	Homozygous	+	+	+	–	–
				15	11	F			+	+	+	–	–
				16	5	F			+	+	–	–	–
This report		Japan	7	17	9	M	W243R	Compound heterozygous	+	+	+	–	+
				18	16	M	Del (I340_R366)		+	+	+	–	+

our patients demonstrated a new clinical feature, lung adenocarcinoma with mental retardation and minor malformations.

The mutations we detected were novel and have not been reported in the earlier cases. The mutation c.727 T>C generates mutant protein with an amino acid substitution of W243R. The mutation g.24994 G>A located 5bp after exon 10 generated a protein that was missing 27 amino acids of exon 10.

These mutations are likely to have crucial influence on the function of MRE11, because they are within the nuclease domain (MRE11 motif IV) and close to the DNA binding domain (407-421), respectively. This *MRE11* gene alteration may be related to the phenotype of our patients: the early onset and rapid progression of the disease, the development of lung adenocarcinoma, and the presence of mental retardation with minor malformations.

In 1995, the *MRE11* gene was isolated by Petrini et al.[4] The gene is consisted of 20 exons and located at 11q21. MRE11 protein interacts with RAD50 and NBS1 proteins and forms a core of MRN complex. The MRN complex is important for double-strand break repair, meiotic recombination, and telomere maintenance.[5] The complex acts not only as a transducer of the signal from activated ATM protein, but also as a stimulator of ATM protein in the early phase of the double-strand break response.[6] These studies explain the clinical and biological resemblance among A-T, NBS, and ATLD.

A-T is well known as a disorder with predisposition to malignancy such as lymphoid tumor and several types of adenocarcinoma.[7,8] The lifetime prevalence of cancer in patients with A-T is 10% to 30%. NBS is also known as a disorder with predisposition to malignancy of the lymphoid organ.[9] In these disorders, increased frequency of tumors can be explained by increased genome instability. The genomic instability arises from defective recognition and repair of double-strand DNA breaks and from defective cell cycle checkpoints. Although these disorders share common clinical features as a genomic instability syndrome, there has been no report of malignancy in patients with ATLD. Association of *MRE11* mutations/polymorphisms with lung adenocarcinoma has not been reported, and insufficient data is available to assess the role of genetic change of *MRE11* in cancer and cancer risk at this point.

Although further detailed biochemical study is required for delving into the pathogenesis of lung carcinoma in our patients with MRE11 deficiency, this report suggests a possible risk of malignancy associated with *MRE11* genotype in patients with ATLD. ■

Submitted for publication Oct 24, 2008; last revision received Jan 15, 2009; accepted Feb 17, 2009.

Reprint requests: Tomohiro Morio, MD, PhD, 1-5-45 Yushima, Bunkyo-ku, Tokyo 113-8519, Japan. E-mail: tmorio.ped@tmd.ac.jp.

References

1. Stewart GS, Maser RS, Stankovic T, Bressan DA, Kaplan MI, Jaspers NG, et al. The DNA double-strand break repair gene hMRE11 is mutated in individuals with an ataxia-telangiectasia-like disorder. Cell 1999;99: 577-87.
2. Delia D, Piane M, Buscemi G, Savio C, Palmeri S, Lulli P, et al. MRE11 mutations and impaired ATM-dependent responses in an Italian family with ataxia-telangiectasia-like disorder. Hum Mol Genet 2004;13: 2155-63.
3. Fernet M, Gribaa M, Salih MA, Seidahmed MZ, Hall J, Koenig M. Identification and functional consequences of a novel MRE11 mutation

affecting 10 Saudi Arabian patients with the ataxia telangiectasia-like disorder. Hum Mol Genet 2005;14:307-18.
4. Petrini JH, Walsh ME, DiMare C, Chen XN, Korenberg JR, Weaver DT. Isolation and characterization of the human MRE11 homologue. Genomics 1995;29:80-6.
5. Carney JP, Maser RS, Olivares H, Davis EM, Le Beau M, Yates JR III, et al. The hMre11/hRad50 protein complex and Nijmegen breakage syndrome: linkage of double-strand break repair to the cellular DNA damage response. Cell 1998;93:477-86.
6. Uziel T, Lerenthal Y, Moyal L, Andegeko Y, Mittelman L, Shiloh Y. Requirement of the MRN complex for ATM activation by DNA damage. EMBO J 2003;22:5612-21.
7. Hecht F, Hecht BK. Cancer in ataxia-telangiectasia patients. Cancer Genet Cytogenet 1990;46:9-19.
8. Taylor AM, Metcalfe JA, Thick J, Mak YF. Leukemia and lymphoma in ataxia telangiectasia. Blood 1996;87:423-38.
9. The International Nijmegen Breakage Syndrome Study Group. Nijmegen breakage syndrome. Arch Dis Child 2000;82:400-6.

The Journal of Immunology

Impaired CD4 and CD8 Effector Function and Decreased Memory T Cell Populations in ICOS-Deficient Patients

Naomi Takahashi, Kenji Matsumoto, Hirohisa Saito, Toshihiro Nanki, Nobuyuki Miyasaka, Tetsuji Kobata, Miyuki Azuma, Sang-Kyou Lee, Shuki Mizutani and Tomohiro Morio

J. Immunol. 2009;182;5515-5527
doi:10.4049/jimmunol.0803256
http://www.jimmunol.org/cgi/content/full/182/9/5515

The Journal of Immunology is published twice each month by The American Association of Immunologists, Inc., 9650 Rockville Pike, Bethesda, MD 20814-3994.

Print ISSN: 0022-1767 Online ISSN: 1550-6606.

Impaired CD4 and CD8 Effector Function and Decreased Memory T Cell Populations in ICOS-Deficient Patients

Naomi Takahashi,* Kenji Matsumoto,† Hirohisa Saito,† Toshihiro Nanki,‡ Nobuyuki Miyasaka,‡ Tetsuji Kobata,§ Miyuki Azuma,¶ Sang-Kyou Lee,‖ Shuki Mizutani,* and Tomohiro Morio[1]*

Interaction of ICOS with its ligand is essential for germinal center formation, T cell immune responses, and development of autoimmune diseases. Human ICOS deficiency has been identified worldwide in nine patients with identical ICOS mutations. In vitro studies of the patients to date have shown only mild T cell defect. In this study, we report an in-depth analysis of T cell function in two siblings with novel ICOS deficiency. The brother displayed mild skin infections and impaired Ig class switching, whereas the sister had more severe symptoms, including immunodeficiency, rheumatoid arthritis, inflammatory bowel disease, interstitial pneumonitis, and psoriasis. Despite normal CD3/CD28-induced proliferation and IL-2 production in vitro, peripheral blood T cells in both patients showed a decreased percentage of CD4 central and effector memory T cells and impaired production of Th1, Th2, and Th17 cytokines upon CD3/CD28 costimulation or PMA/ionophore stimulation. The defective polarization into effector cells was associated with impaired induction of T-bet, GATA3, MAF, and retinoic acid-related orphan nuclear hormone receptor (RORC). Reduced CTLA-4$^+$CD45RO$^+$FoxP3$^+$ regulatory T cells and diminished induction of inhibitory cell surface molecules, including CTLA-4, were also observed in the patients. T cell defect was not restricted to CD4 T cells because reduced memory T cells and impaired IFN-γ production were also noted in CD8 T cells. Further analysis of the patients demonstrated increased induction of receptor activator of NF-κB ligand (RANKL), lack of IFN-γ response, and loss of Itch expression upon activation in the female patient, who had autoimmunity. Our study suggests that extensive T cell dysfunction, decreased memory T cell compartment, and imbalance between effector and regulatory cells in ICOS-deficient patients may underlie their immunodeficiency and/or autoimmunity. *The Journal of Immunology,* **2009, 182: 5515–5527.**

Members of the CD28 family play an important role in the regulation of T cell immune responses (1, 2). Expression of these molecules and their ligands is tightly regulated to deliver either costimulatory or inhibitory signals (2–5), and their uncoordinated regulation leads to the development of immunological disorders (6–8).

ICOS (CD278) is a costimulatory member of the CD28 family, and its expression is induced in CD4 T cells upon activation (9–11). The ICOS signal is induced by interaction with its partner, the ICOS ligand (ICOS-L[2]; CD275), a molecule highly expressed on B cells and dendritic cells and weakly on T cells and nonlymphoid cells (1, 12). Signaling through ICOS enhances T cell proliferation, secretion of cytokines, and up-regulation of cell surface molecules (11, 13, 14).

Previous research has showed that the ICOS-ICOS-L interaction is important for productive T-B cell coactivation, CD40-mediated Ig class switch recombination, and development of Th2 immune responses (1, 15–17). Induction of the Th1 cytokine IFN-γ is relatively unaffected and in some studies augmented; other studies have documented the importance of ICOS in Th1 responses (15, 16, 18–21). Accumulating evidence indicates that ICOS also regulates the generation of Th17 cells, differentiation of FoxP3$^+$ regulatory T cells (Tregs), and homeostatic survival of invariant NKT (iNKT) cells (22–24).

Although earlier investigations of ICOS-null mice revealed normal numbers of naive/memory T cells and normal primary clonal expansion and survival of memory T cells, more recent investigation has demonstrated lower numbers of effector memory T cells (TEMs) in ICOS$^{-/-}$ mice in the steady state (23). Seemingly contradictory results have been reported on the requirement of ICOS for T cell differentiation and function.

Most studies have depicted ICOS as a costimulator. Indeed, the blockade of the ICOS-ICOS-L interaction abrogates the development of murine models of autoimmune diseases, as follows: rheumatoid arthritis (RA), inflammatory bowel disease (IBD), myasthenia gravis, type I diabetes mellitus, experimental myositis, autoimmune carditis, and graft-vs-host disease (25–30).

Previously, human ICOS deficiency has been reported in nine patients from four families (31–33). Importantly, the same homologous genetic deletion of exons 2 and 3 was identified in all patients, indicating a founder effect in all four families. Analysis of these patients revealed reduced numbers of memory B cells and pan-hypoimmunoglobulinemia, but no impairment in the secretion of TNF-α, IFN-γ, IL-2, IL-4, IL-10, or IL-13. Normal surface

*Department of Pediatrics and Developmental Biology, Graduate School of Medical and Dental Sciences, Tokyo Medical and Dental University, Tokyo, Japan; †Department of Allergy and Immunology, National Research Institute for Child Health and Development, Tokyo, Japan; ‡Department of Medicine and Rheumatology, Graduate School of Medical and Dental Sciences, Tokyo Medical and Dental University, Tokyo, Japan; §Department of Immunology, Dokkyo Medical University, Tochigi, Japan; ¶Department of Molecular Immunology, Graduate School of Medical and Dental Sciences, Tokyo Medical and Dental University, Tokyo, Japan; and ‖Department of Biotechnology, Yonsei University, Seoul, Korea

Received for publication October 6, 2008. Accepted for publication February 24, 2009.

The costs of publication of this article were defrayed in part by the payment of page charges. This article must therefore be hereby marked *advertisement* in accordance with 18 U.S.C. Section 1734 solely to indicate this fact.

[1] Address correspondence and reprint requests to Dr. Tomohiro Morio, Tokyo Medical and Dental University Graduate School of Medicine, 1-5-45 Yushima, Bunkyo-Ku, Tokyo 113-8519, Japan. E-mail address: tmorio.ped@tmd.ac.jp

[2] Abbreviations used in this paper: ICOS-L, ICOS ligand; IBD, inflammatory bowel disease; IP, interstitial pneumonitis; RA, rheumatoid arthritis; RE, relative expression; TCM, central memory T cell; TEM, effector memory T cell; Treg, regulatory T cell; BTLA, B and T lymphocyte attenuator; EOMES, eomesodermin; PD-1, programmed death-1; RANKL, receptor activator of NF-κB ligand; RORC, retinoic acid-related orphan nuclear hormone receptor.

www.jimmunol.org/cgi/doi/10.4049/jimmunol.0803256

expression of CD69, CD40L (CD154), CD25, and OX40 (CD134) was observed on their T cells following stimulation (31). A later study provided evidence of defects in IL-10 and IL-17 production (33); however, no major impairment of T cell function was demonstrated. Autoimmunity, manifested as autoantibody-mediated neutropenia, was observed in only one patient (33). Although there have been reports on the effects of ICOS on CD8 responses in mice (34, 35), impact of ICOS on CD8 T cells is not yet completely understood.

In this study, we describe the case of two siblings having ICOS deficiency with a novel mutation in the ICOS gene. Although both patients displayed varing degrees of immunodeficiency, only the sister showed a wide range of autoimmune diseases, including RA, IBD, interstitial pneumonitis (IP), and psoriasis.

In this study, we focused on the T cell immune function of these ICOS-deficient patients. Detailed analysis demonstrated a reduction in memory T cells and a major subtype of Tregs; impaired polarization into Th1, Th2, and Th17; and defective induction of CTLA-4 molecules and other surface inhibitory receptors.

We further assessed activation-induced T cell proliferation and apoptosis, induction of costimulatory receptor molecules, and expression of master regulators for effector T cell subsets, and explored the mechanisms of T cell defect and autoimmunity in these patients using quantitative mRNA analysis.

Materials and Methods

Patients and controls

Patients were diagnosed with common variable immunodeficiency, according to the European Society for Immunodeficiencies criteria (www.esid.org). Twelve healthy volunteers (6 male, 6 female) aged between 26 and 48 years were recruited. The study was approved by the institutional ethical committee of Tokyo Medical and Dental University, and written informed consent was obtained from the patients, the elder sister and mother of the patients, and healthy controls.

Sequencing and RT-PCR of ICOS

Genomic DNA was extracted from peripheral blood using a DNA blood mini kit (Qiagen), according to the manufacturer's instructions. The coding sequences of the five exons and the adjacent intron-exon boundaries of the ICOS gene were amplified with specific primers (sequences are available upon request) from genomic DNA on the basis of ICOS sequences obtained from GenBank database (accession numbers AC103880, AC009965, and AB023135). All PCR products were sequenced using BigDye terminator v3.1 and an ABI Prism 3130 Genetic Analyzer (Applied Biosystems); the sequence data were then analyzed using DNASIS software (Hitachi Software). Total RNA was isolated from stimulated PBMCs using an RNeasy mini kit (Qiagen) and reverse transcribed into cDNA using a Superscript III first-strand synthesis system for RT-PCR (Invitrogen). PCR products were separated by agarose gel electrophoresis.

Monoclonal Abs

We used the following FITC-, PE-, PE Texas Red (ECD)-, or PE cyanin 5.1 (PC5)-conjugated Abs: FoxP3 (236A/E7) from Abcam; IgG1 isotype controls, CD3 FITC, CD3 PE (SK7), CD4 PE (SK3), CD8 FITC, CD8 PE (SK1), CD25 FITC (M-A251), IL-4 PE (3010.211), IFN-γ PE (25723.11), 4-1BB PE (4B4-1), OX40 PE (ACT35), and IL-10 PE (JES3-10F1) from BD Pharmingen; CD3 FITC (UCHT1), CD4 PC5 (13B8.2), CD8 ECD (SFCI21Thy2D3), CD8 FITC (B9.11), CD19 ECD, CD19 PE (J4.119), CD20 FITC (B9E9), CD25 PC5 (B1.49.1), CD28 FITC, CD28 purified (CD28.2), CD45RA FITC (ALB11 and 2H4), CD45RO PE, ECD (UCHL1), CD62L ECD (DREG56), CD69 PE (TP1.55.3), CTLA4 PE (BNI3), streptavidin FITC, streptavidin PC5, and TCR Vβ Repertoire kit from Beckman Coulter (CA); CD27 PE (M-T271) and IgD from DakoCytomation; CD45RO PE (UCHL1), IL-17 FITC (eBio64DEC17), B and T lymphocyte attenuator (BTLA) PE (MIH26), programmed death-1 (PD-1) FITC (MIH4), ICOS-L, ICOSL biotin (MIH12), and ICOS FITC (ISA-3) from eBioscience; receptor activator of NF-κB (RANK) PE (9A725) from Imgenex; CD25 PE (4E3) from Miltenyi Biotec; Alexa Fluor 488 goat anti-mouse IgG Ab from Molecular Probes; CCR7 FITC (150503) from eBioscience; and CD3 purified (OKT3) from Janssen Pharmaceutical.

Cell separation and stimulation

PBMCs were isolated from heparinized blood using Lymphoprep (Axis-Shield), as described previously (36). CD4 T cells were negatively selected from the PBMCs using a StemSep device (StemCell Technologies). Thus, the purity of the collected CD4 T cell population was generally >95%. CD8 T cells were prepared with the same technique yielding >90% pure CD8 T cell population. Separated cells were resuspended in RPMI 1640 (WAKO) supplemented with 10% heat-inactivated FBS (Gemini Biological Products), and incubated at 10^6 cells/ml in 24-well plates (Greiner Bioscience) with or without stimulants. For stimulation, we used anti-CD28 mAb (at 1 μg/ml) with plate-bound anti-CD3 mAb or 50 ng/ml PMA (Sigma-Aldrich) plus 1 μg/ml ionomycin (Sigma-Aldrich). The cells were incubated in the medium at 37°C in 5% CO_2 for the indicated time periods. IL-2 (Lymphotec) was used at 700 IU/ml with plate-bound anti-CD3 when assessing ICOS expression.

Flow cytometric analysis

PBMCs, CD4 T cells, or CD8 T cells were stained with the indicated Abs and were analyzed using a FACSCalibur flow cytometer and CellQuest software (BD Biosciences) or an EPICS XL flow cytometer and EXPO32 software (Beckman Coulter), as described previously (37). For intracellular cytokine detection, PBMCs were stimulated with PMA and ionomycin in the presence of GolgiPlug (BD Pharmingen) or brefeldin A (eBioscience) for 5–8 h at 37°C in 5% CO_2. After stimulation, the cells were fixed and permeabilized using a Cytofix/Cytoperm Plus fixation/permeabilization kit (BD Pharmingen). The same permeabilization technique was used to detect CTLA-4 expression. A CellTrace CFSE cell proliferation kit (Molecular Probes) was used for the CFSE assay, and an annexin V FITC/7-AAD kit (Beckman Coulter) for the apoptosis assay.

Cytokine production assay

Negatively selected CD4 T cells or CD8 T cells were incubated with or without stimulants (plate-bound anti-CD3 mAb and anti-CD28 mAb or 50 ng/ml PMA, and 200 nM ionomycin). The supernatants were collected after 24 h and analyzed using ELISA for IL-17, IL-12p40, IL-22, and TGF-β1 (R&D Systems); IL-21 (eBioscience); and human Th1/Th2 cytokines (IFN-γ, IL-2, IL-4, IL-5, IL-6, IL-10, TNF-α, and TNF-β) using a FlowCytomix kit (Bender MedSystems), according to the manufacturer's instructions. All assays were performed in duplicate.

Real-time quantitative PCR

Total RNA was extracted using an RNeasy mini kit with DNase (Qiagen) and reverse transcribed using random hexamer primers and Superscript III reverse transcriptase (Invitrogen). Real-time quantitative PCR was performed using a 7300 Real-Time PCR system (Applied Biosystems) using an assay-on-demand Taqman probe and primers (Hs00174383 for *IL17A*, Hs00243522 for *RANKL*, Hs00203958 for *FOXP3*, Hs00226053 for *RNF128*, Hs00909784 for *CBLB*, Hs00395208 for *ITCH*, Hs00172872 for *EOMES*, Hs00193519 for *MAF*, Hs00231122 for *GATA3*, Hs00894392 for *TBX21*, Hs01076112 for *RORC*, Hs99999901 for *18S*, and Hs99999905 for *GAPDH*), according to the manufacturer's instructions. Relative expression levels of these genes were normalized according to *GAPDH* or *18S rRNA* expression, using a standard curve method as described by the manufacturer. All samples and standards were tested in duplicate.

Oligonucleotide microarray assay

Oligonucleotide microarray assay was conducted with total RNA extracted from a total of 1–3 × 10^6 CD4 T cells stimulated in anti-CD3-coated plates in the presence of anti-CD28 mAb or from unstimulated CD4 T cells, as described previously (38). Data analysis, selection of significant signals, and comparison of the data from multiple samples were conducted, as previously described (38). The results have been deposited in the Gene Expression Omnibus at http://www.ncbi.nlm.nih.gov/geo/(accession number GSE12875).

Results

Clinical course of patients and diagnosis of ICOS deficiency

The sister, hereafter designated patient 1, was born in 1967. In her infancy, she had episodes of prolonged viral infection. In 2001, when she developed a pulmonary abscess following appendectomy, she was diagnosed with common variable immunodeficiency according to the European Society for Immunodeficiencies criteria (at the age of 34), and i.v. Ig treatment was started to

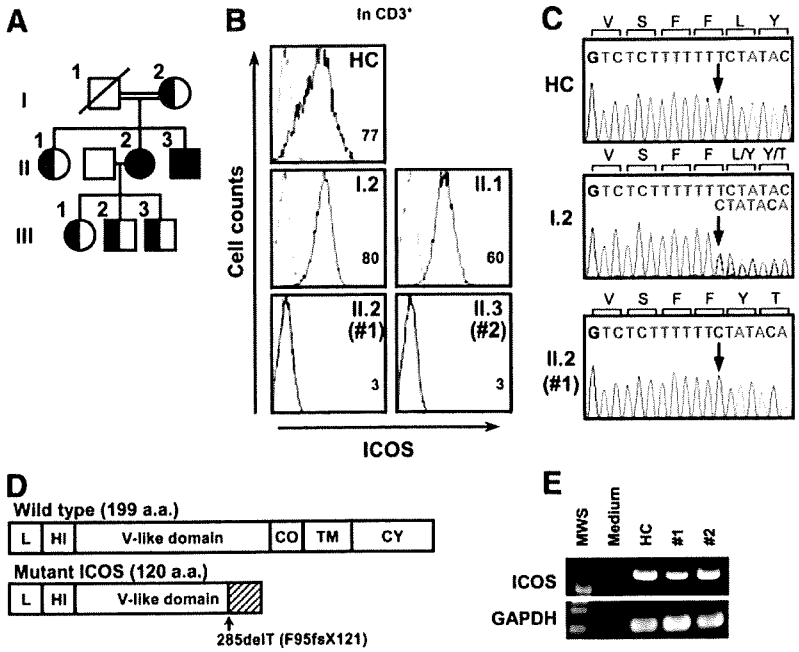

FIGURE 1. Diagnosis of ICOS deficiency. *A*, Pedigree of the ICOS deficiency patients. Filled symbols represent affected family members (II.2, patient 1; II.3, patient 2). The patients were products of a consanguineous marriage. *B*, Expression of ICOS. PBMCs from patients 1 and 2, their mother (I.2), elder sister (II.1), and a healthy control (HC) were cultured on an anti-CD3 mAb-coated plate in the presence of IL-2 and stained with anti-ICOS mAb (solid line) or control mAb (dotted line). The graphs are gated on CD3 T cells. Mean fluorescence intensity of ICOS is shown in each graph. *C*, Partial sequences of exon 2 of *ICOS* from HC, the mother of the patients, and patient 1. The elder sister of the patients had a heterozygous mutation that was detected in the mother, and the brother (patient 2) had a homozygous mutation at codon 285. *D*, Schematic figure showing the wild-type 199-aa ICOS protein and putative 120-aa mutant ICOS protein obtained from the patients. The shaded area represents the mutant proteins generated by induction of a frameshift at codon 285. L, L region; HI, hydrophilic region; CO, connecting region; TM, transmembrane region; CY, cytoplasmic region. *E*, RT-PCR analysis for *ICOS* mRNA. *ICOS* mRNA (1–597) from anti-CD3/IL-2-stimulated PBMCs from patient 1 (#1) and patient 2 (#2), and HC was amplified by RT-PCR with specific primers. The PCR product was analyzed by agarose gel electrophoresis. MWS, m.w. standard.

maintain the trough IgG level of >4 g/L. In the following years, she developed psoriasis-like cutaneous lesions and arthritis in multiple joints, including bilateral shoulder, wrist, knee, metacarpophalangeal, proximal interphalangeal, and metatarsophalangeal joints. RA was diagnosed on the basis of the findings of proliferative synovitis of multiple finger and toe joints with erosive changes on x-ray examination. Psoriatic arthritis was ruled out based on the joints affected and the x-ray findings. In 2003, she developed abdominal colic, diarrhea, and IP, and had a constantly elevated serum CRP level. Diagnosis of IBD was made upon biopsy of the colon, and both IBD and IP were controlled by prednisolone. She was referred to our hospital in 2006. Methotrexate at 8 mg/week significantly improved not only the articular signs and symptoms of RA, but also the psoriatic skin changes and IBD. The dose of prednisolone was successfully tapered from 15 to 8 mg/day. Since then, she has been on regular Ig supplementation every 2 wk.

The pedigree of the patient is shown in Fig. 1*A*. The patient had two siblings: her sister was healthy with no immunological abnormalities, whereas her younger brother (hereafter designated patient 2) developed occasional skin abscesses and mild psoriasis-like cutaneous lesions, and had slightly low levels of IgG (611 mg/dL) when examined at the age of 35. The serum IgG level stays at the same level to date; and he is not yet on Ig supplementation.

A summary of the immunological data of patients 1 and 2, the elder sister, and ICOS deficiency patients reported to date (33) is given in Table I. Patient 1 had a slightly reduced B cell count, whereas patient 2 had a normal B cell count. In both siblings, however, $CD27^+IgD^-$-switched memory B cells were virtually absent in the peripheral blood samples (Table I). The serum samples contained no detectable specific IgG Abs against measles, mumps, or rubella viruses despite a previous record of vaccine inoculation (data not shown). The immunological parameters of patient 2 are unique in that he showed elevated serum IgM (456 mg/dL). The T cells of the patients displayed abundant expression of CD69 and HLA-DR when stimulated via TCRs in the presence of exogenous IL-2 (data not shown), but lacked surface ICOS expression (Fig. 1*B*). Activated T cells from the mother (I.2) and elder sister (II.1) displayed normal ICOS induction.

Sequencing of the ICOS gene revealed the homozygous deletion of T at codon 285, which caused a frameshift in the coding region of ICOS and introduced a premature stop codon at aa 121 (F95fsX121) in the patients (Fig. 1, *C* and *D*).

Sequencing analysis of the *ICOS* gene in the elder sister and mother demonstrated a heterozygous mutation (Fig. 1*C*). RT-PCR of *ICOS* mRNA with specific primers amplifying the entire coding region of the *ICOS* gene (1–597) demonstrated the presence of an *ICOS* transcript, suggesting the absence of nonsense-mediated RNA decay (Fig. 1*E*).

Decreased memory T cells in ICOS-deficient patients

A previous report on human ICOS-deficient patients showed a normal distribution of naive, memory, and effector T cells (31, 33, 39). However, as seen in the representative FACS plots in Fig. 2*A*, we observed a substantial reduction in $CD4^+CD45RO^+$ memory cells in the patients compared with age- and gender-matched controls (12.1 and 6.6% for patients 1 and 2, respectively, and 24.5

Table I. *Summary of immunological data*[a]

	Patient 1	Patient 2	Previously Reported ICOS-Deficient Patients (range)	II.1 (hetero)	Normal Range
Lymphocytes (/mm^3)	1,400 ± 200	1,900 ± 200	353–4,153	1,400	1,200–2,800
Immunophenotype of PBMCs (%)					
CD3	80.5 ± 5.0	72.4 ± 2.0	70.4–95.6	71.7	58–84
CD4	59.5 ± 5.0	55.6 ± 3.0	23.1–59.2	50.5	25–58
CD8	24.1 ± 4.0	19.1 ± 3.0	16.6–64.0	22.5	18–46
CD16	7.8 ± 0.2	11.2 ± 2.0	–	14.5	6–25
CD19	2.1 ± 0.6	4.8 ± 0.5	0.6–21.2	9.7	3–20
CD19$^+$CD27$^+$(%Bc)	0.2	0.8	2.0–12.6	11.4	8–35
CD19$^+$CD27$^+$IgD$^-$(%Bc)	0	0.4	0.0–1.3	8.6	7–32
Blastogenesis (cpm)					
PHA	56,100	45,600	78,900–95,700	–	20,500–56,800
Con A	45,300	32,500	–	–	20,300–65,700
Igs					
IgG (mg/dL)	315	611		1,025	900–1,600
IgG1	–	322	2.8–181	–	
IgG2	–	365	10–71.7	–	
IgG3	–	19.5	4–44.9	–	
IgG4	–	< 3.0	0–7	–	
IgM (mg/dL)	56	456	20–180	143	40–250
IgA (mg/dL)	46	103	6–58	137	100–250
IgE (IU/L)	<5	<5	17.5–38	ND	<173

[a] Immunological data of patients 1 and 2 are summarized. Lymphocyte counts and immunophenotyping of PBMCs were performed on more than three separate occasions; these are expressed as mean ± SD. Ig levels shown are those obtained at diagnosis (before Ig supplementation). Data from previous reported ICOS deficiency (33) and data from the elder sister of the patients are also shown. %Bc: % in B cells.

and 28.9% for controls 1 and 2, respectively). This reduction was seemingly counterbalanced by an increased frequency of naive T cells.

Gated CD4 memory T cells from PBMCs were further analyzed for CCR7 and CD62L expression to define CCR7$^+$-CD62L$^+$CD45RO$^+$ central memory T cells (TCMs) and

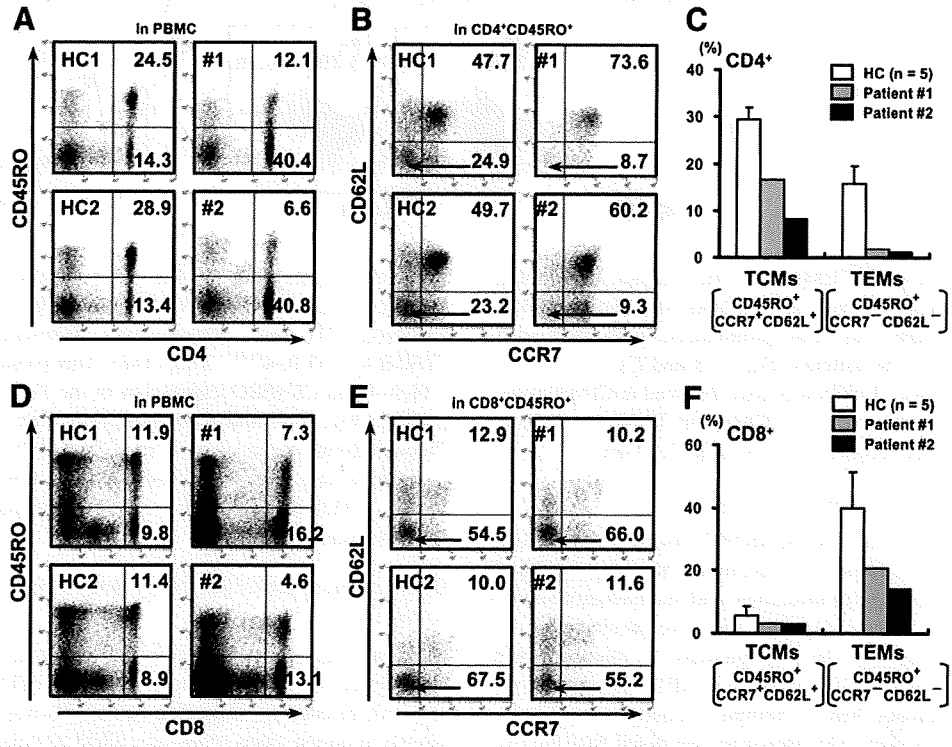

FIGURE 2. Decrease in memory T cells in ICOS-deficient patients. PBMCs from healthy controls (HC) and ICOS-deficient patients (1 and 2) were analyzed for the frequency of memory T cells. PBMCs were stained with Abs to CD4 or CD8, CD45RO, CCR7, and CD62L to assess memory T cell subsets (*A–F*). *A* and *D*, Representative CD4/CD45RO (*A*) and CD8/CD45RO (*D*) dot blots. Values shown in *upper* and *lower right quadrants* indicate percentages of the cells among total PBMCs. *B* and *E*, TCMs (CCR7$^+$CD62L$^+$) and TEMs (CCR7$^-$CD62L$^-$) in the memory CD4 T cell fraction (*B*) and in the memory CD8 T cell fraction (*E*). Values indicate frequencies of TCMs and TEMs in the CD4$^+$CD45RO$^+$ population or in the CD8$^+$CD45RO$^+$ population. Representative FACS analyses for healthy controls (HC) and patients are shown. *C* and *F*, Summary of percentages of TCMs and TEMs among CD4 T cells (*C*) and CD8 T cells (*F*). A □ with error bar represents the mean ± SD values of the indicated subsets from five healthy controls. Mean percentage for the respective subsets from two independent experiments is shown for the patients.

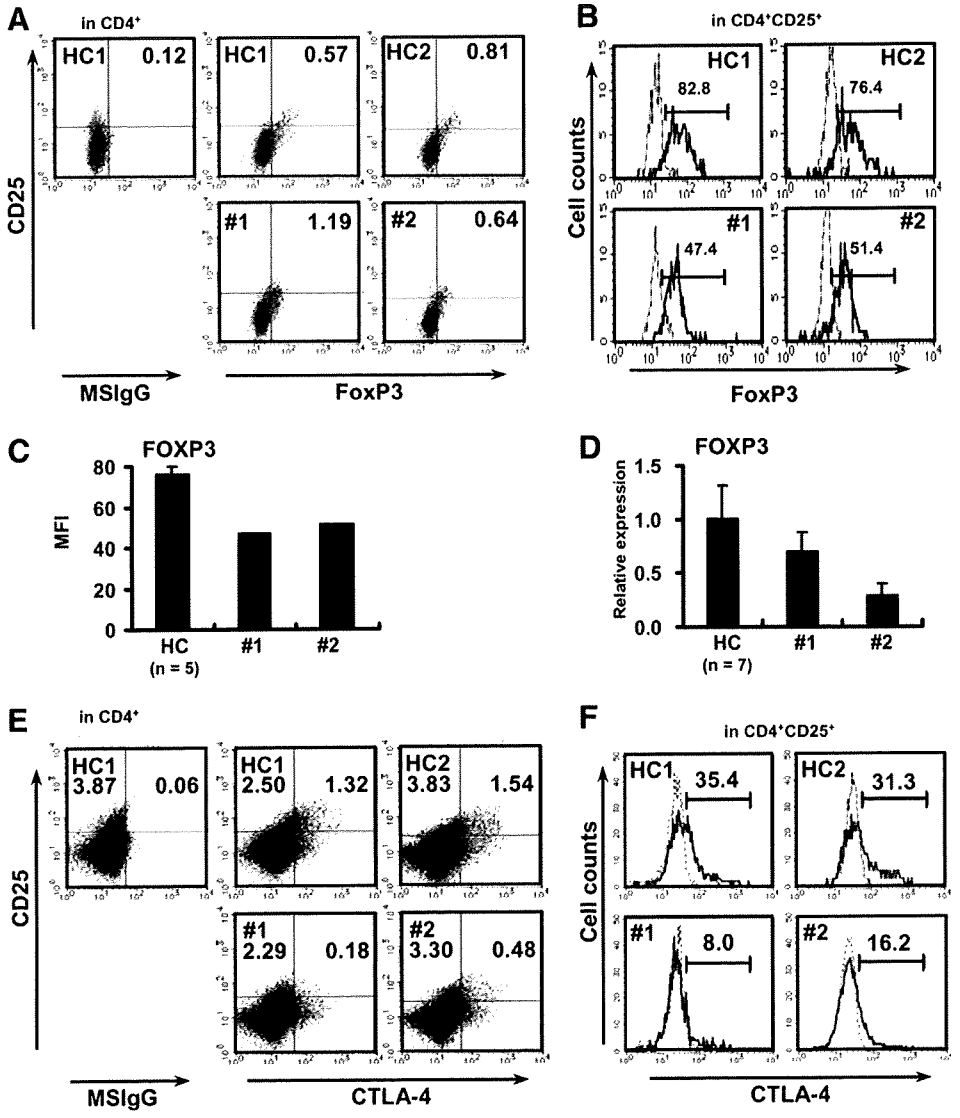

FIGURE 3. Decrease in CTLA-4$^+$ Treg subset in ICOS-deficient patients. *A*, Flow cytometric analysis of intracellular Foxp3 expression in CD4$^+$CD25$^+$ T cells. Numbers in dot plots are percentages of CD25$^+$-Foxp3$^+$ cells among CD4$^+$ T cells. *B*, Mean fluorescence intensity (MFI) of FoxP3 in CD4$^+$CD25$^+$ cells. FoxP3 expression in CD4$^+$CD25$^+$ cells is shown as a contour plot. MFI of FoxP3 is shown in the *upper right quadrant*. *C*, Summary of MFI of FoxP3 in CD4$^+$CD25$^+$ cells. *D*, Quantitative real-time PCR analysis for FoxP3 gene expression. mRNA expression levels in purified CD4 T cells were calculated with 18S rRNA as a reference, and the relative expression in healthy controls (HC) was adjusted to 1.0. Error bar indicates SD for HC and SEM for patients 1 and 2. *E* and *F*, Expression of CTLA-4 Ag in CD4$^+$CD25$^+$ T cells. Numbers indicate frequencies of CTLA-4$^+$ and CTLA-4$^-$ Treg subsets among CD4$^+$ T cells. PBMCs from five HC were analyzed by FACS. FACS analysis was performed three times for the patients. Representative dot plots (*E*) and contour plots (*F*) are shown. MFI of CTLA-4 in CD4$^+$CD25$^+$ Treg cells is indicated in the plots (*F*).

CCR7$^-$CD62L$^-$CD45RO$^+$ TEMs (40). The analysis showed that compared with controls, the patients had 2- to 5-fold fewer TCMs. The reduction in TEMs was more pronounced, with more than 6-fold fewer TEMs in the patients (Fig. 2, *B* and *C*).

A decrease in memory T cells was also observed in CD8 T cells. We observed a reduction in both TCMs and TEMs in patients compared with control subjects ($n = 5$) (Fig. 2, *D–F*).

Decreased Tregs in ICOS-deficient patients

Most Tregs express ICOS, and ICOS^{high+} Tregs preferentially produce IL-10 (41). In addition, recent studies have demonstrated the importance of ICOS in proliferation and maintenance of the pool size of FoxP3$^+$ Tregs (41). We therefore investigated the frequency of Treg cells in the two patients by staining their PBMCs for CD4, CD25, and intracellular FoxP3. Contrary to our predictions, the patients had a normal proportion of CD4$^+$ CD25$^+$FoxP3$^+$ Tregs (Fig. 3*A*). However, we noted that the expression level of FoxP3, as reflected by the mean fluorescence intensity, was diminished in both patients (Fig. 3, *B* and *C*). To ascertain the low FoxP3 expression obtained in the FACS analysis, we evaluated the level of FoxP3 mRNA in a real-time PCR assay. This showed a marked reduction in FoxP3 expression in patient 2 and a slight decrease in patient 1 compared with the normal subjects ($n = 7$) (Fig. 3*D*).

Recent studies have shown that human CD4$^+$CD25$^+$FoxP3$^+$ Tregs comprise two subsets, as follows: IL-10-producing ICOS$^+$ CD45RO$^+$CTLA-4$^+$ Tregs and TGF-β-producing ICOS$^-$ CD45RA$^+$CTLA-4^{dull+} Tregs (42). This prompted us to examine CTLA-4 and CD45RO expression in the Tregs of ICOS-deficient patients. Fig. 3, *E* and *F*, demonstrates that most CD4$^+$CD25$^+$ Tregs in these patients were of the CTLA-4^{dull+} or CTLA-4$^-$ subpopulation and expressed CD45RA (data not shown), indicating that the CTLA-4$^+$ subset of Tregs that potentially produces IL-10 was severely decreased.

Defective induction of inhibitory molecules in ICOS-deficient patients

ICOS-null mice showed defective CD40-mediated Ig class switching because of lack of effective CD40L (CD154) up-regulation (15, 16). In contrast, induction of CD40L was normal in the previously reported cases of human ICOS deficiency (33). Up-regulation of 4-1BB (CD137), BTLA (CD272), and CTLA-4 (CD152) was normal in ICOS knockout mice (23), as was that of OX40 (CD134) and CTLA-4 in patients with ICOS deficiency in a previous study (31).

We estimated the expression of these costimulatory and inhibitory receptors on ICOS$^{-/-}$ T cells. PBMCs from controls and patients were stimulated with PMA/ionophore (data not shown) or anti-CD3/

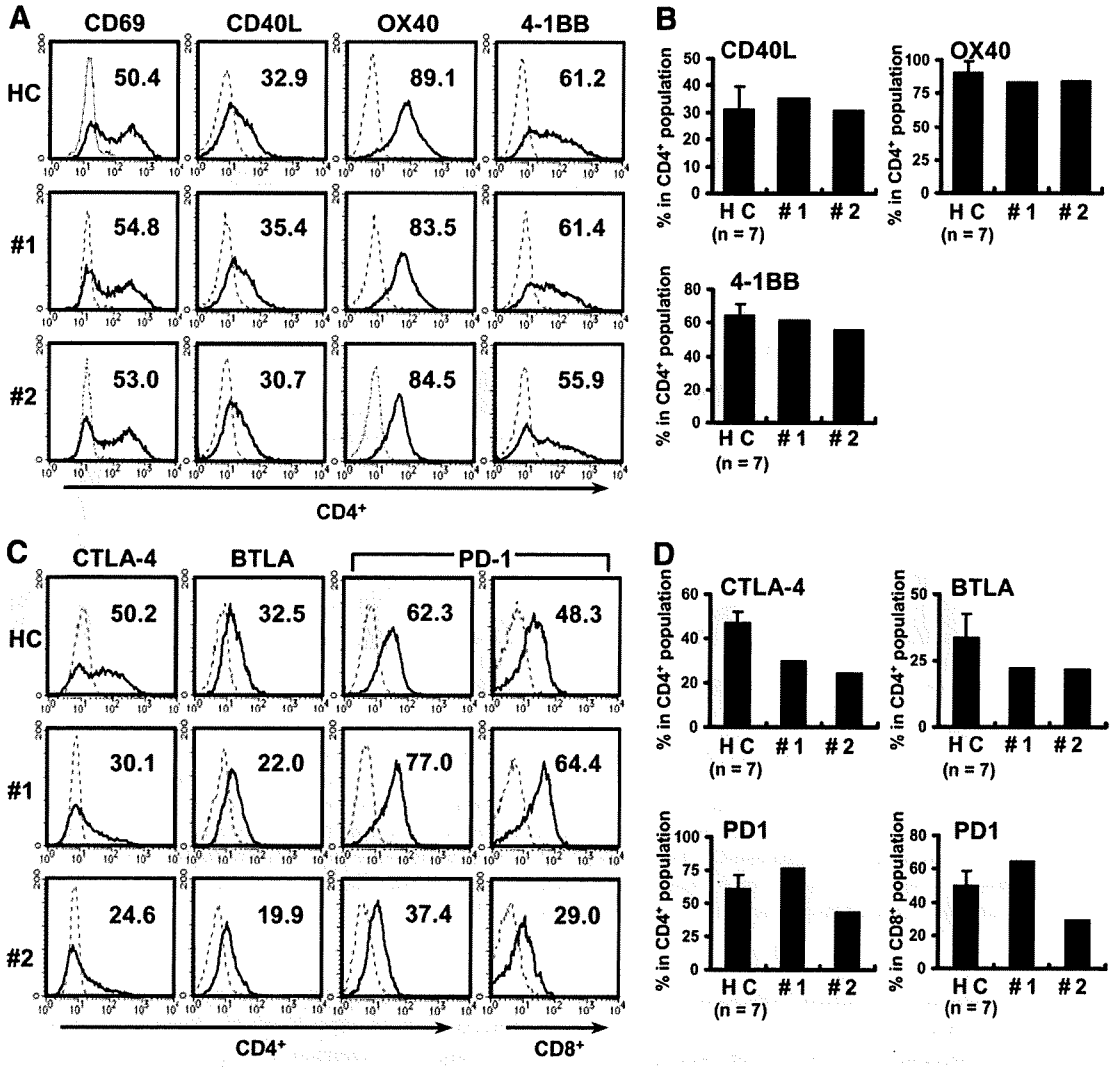

FIGURE 4. Induction of costimulatory and inhibitory molecules in ICOS-deficient patients. *A*, Induced expression of CD40L, OX40, and 4-1BB. PBMCs from healthy controls (HC) and ICOS-deficient patients (#1 and #2) were stimulated with plate-bound anti-CD3 mAb and anti-CD28 mAb for 48 h and analyzed for CD40L, OX40, and 4-1BB expression by FACS. CD69 expression was monitored as an indicator of cell activation. Numbers indicate percentages of the cell population positive for the indicated Ags among CD4 T cells. A contour plot from one representative control of seven HC is shown for each subset. A dotted line indicates a control staining with isotype-matched Ab. *B*, Summary of frequencies of CD40L, OX40, and 4-1BB in CD4 T cells stimulated as in *A* from HC ($n = 7$) and patients 1 and 2. FACS analysis was performed twice for the patients, and average percentages were plotted. Error bar indicates SD. *C*, Induction of CTLA-4, BTLA, and PD-1. PBMCs were stimulated with plate-bound anti-CD3 mAb and anti-CD28 mAb for 48 h. Cells were stained with Abs to CTLA-4, BTLA, and PD-1 together with anti-CD4 mAb or anti-CD8 mAb. Numbers indicate percentages of cell population positive for indicated Ags among CD4 or CD8 T cells. FACS analysis from one representative control of seven HC is shown for each subset. A dotted line indicates a control staining with isotype-matched Ab. *D*, Pooled data from HC ($n = 7$) and patients (1 and 2). Percentages of CTLA-4$^+$, BTLA$^+$, and PD1$^+$ CD4 T cells among CD4 T cells and that of PD-1$^+$ CD8 T cells among CD8 T cells from HC and ICOS-deficient patients (1 and 2) after CD3/CD28 stimulation are shown. The FACS analysis was conducted three times for the patients, and average percentages were plotted. Error bar indicates SD.

anti-CD28, and the cells were examined at the end of incubation for the expression of TNF/TNFR family proteins (TNFRI (CD120a), TNFRII (CD120b), CD40L, OX40, and 4-1BB) and of CD28 family proteins (CTLA-4, BTLA, and PD1 (CD279)).

The analysis revealed that CD40L expression was induced normally in the patients' CD4 T cells, indicating that the hyper-IgM phenotype observed in patient 2 was not due to defective induction of CD40L.

T cells were fully activated in the patients at the end of CD3/CD28 stimulation, as evidenced by CD69 Ag expression. The levels of OX40, 4-1BB, TNFRI, and TNFRII were normal on the surface of the T cells in the ICOS-deficient patients (Fig. 4, *A* and *B*, and data not shown).

Baseline CD28 expression in CD4 T cells was similar to that of healthy subjects (data not shown). In contrast, the frequency of CTLA-4$^+$ CD4 T cells after CD3/CD28 costimulation was markedly reduced in the patients (Fig. 4*C*). Combined data from seven age-matched controls showed that CTLA-4 was induced in 47.4 ± 4.9% of CD4 T cells. In contrast, induction was observed in 30.1 and 24.6% of CD4 T cells in patients 1 and 2, respectively (Fig. 4, *C* and *D*). Moreover, as seen in the representative plot in Fig. 4*C*, the expression level of CTLA-4 in the CTLA-4$^+$ population was also diminished in the patients.

Induction of BTLA, another inhibitory receptor with similarities to CTLA-4 (5), was then estimated. The average percentage of BTLA$^+$ CD4 T cells was slightly lower in the patients (22.0% for

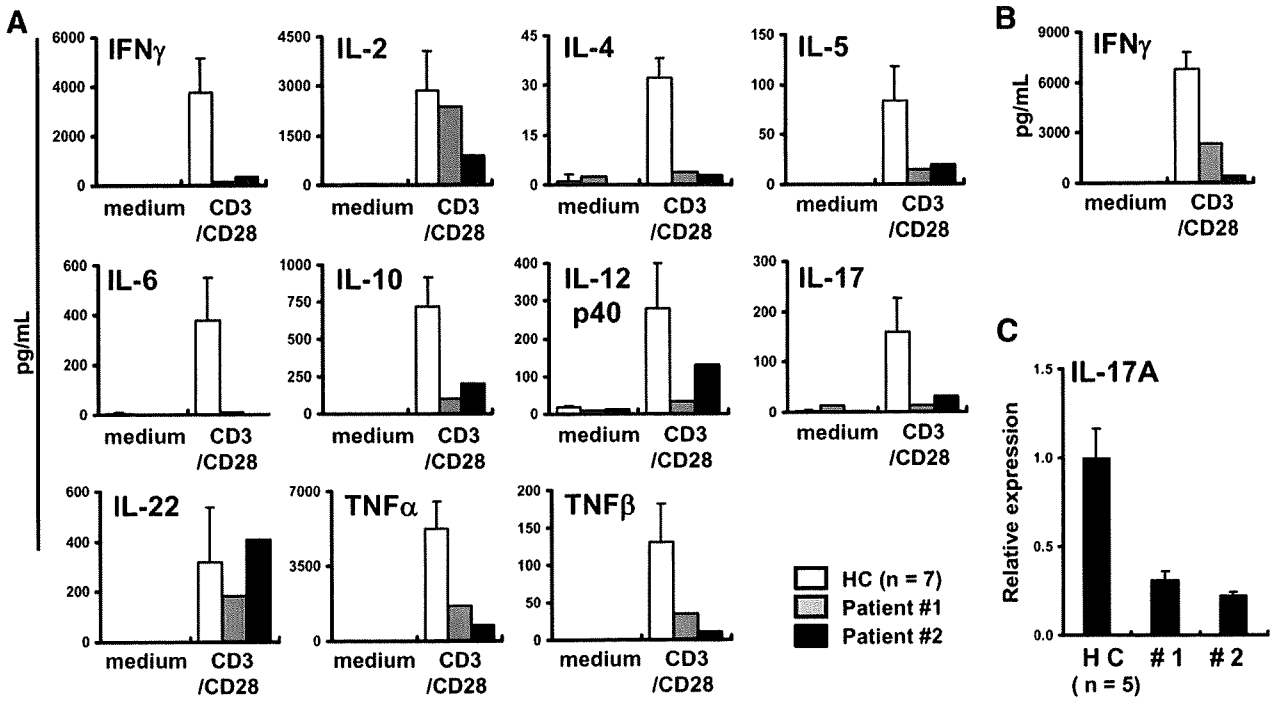

FIGURE 5. Impaired cytokine production in ICOS-deficient patients. *A*, Purified CD4 T cells were stimulated with plate-bound anti-CD3 mAb and anti-CD28 mAb for 24 h or in a medium, and the levels of cytokines in the supernatants were measured by ELISA, FlowCytomix, or both. Error bars for healthy controls (HC, $n = 7$) indicate SD. Experiments were repeated at least twice for the patients, and mean concentrations were plotted. *B*, Purified CD8 T cells were stimulated as in *A*, and the levels of IFN-γ in the supernatants were measured by FlowCytomix. □, HC; ▨, patient 1; ■, patient 2. Error bars for HC ($n = 5$) indicate SD. Experiments were repeated twice for the patients, and mean concentrations were plotted. *C*, IL-17A mRNA expression. The level of IL-17A mRNA was measured in anti-CD3/anti-CD28-stimulated $CD4^+$ T cells by real-time PCR. Relative mRNA level of IL-17A was calculated using GAPDH expression as a reference, and the mean expression level for HC ($n = 5$) was adjusted to 1.0. Error bar indicates SD. IL-17A mRNA expression for the patients was measured three times, and is expressed as mean ± SEM.

patient 1; 21.4% for patient 2) compared with controls (34.0 ± 8.7%, $n = 7$) (Fig. 4, *C* and *D*).

In the patients, the frequency of CD4 T cells bearing PD1, a molecule that plays a critical role in the induction and/or maintenance of T cell tolerance (1), was similar to that in controls (Fig. 4, *C* and *D*). The percentages of $PD1^+$ CD8 T cells, which function as inhibitory T cells (43), were slightly reduced only in patient 2 (29.0%) compared with controls (49.8 ± 9.0%, $n = 7$).

Impaired production of cytokines in ICOS-deficient patients

We next assessed the production of a panel of cytokines by a FlowCytomix bead-based multiplex assay, ELISA, or both, after incubation of CD4 T cells purified to >95% with costimulation of the TCR-CD3 complex via CD28.

In contrast to previous data obtained in other cases of human ICOS deficiency, the production of IFN-γ (Th1 cytokine) and IL-4 and IL-5 (Th2 cytokines) was significantly reduced (Fig. 5*A*) in the patients than in controls (31, 33). Secretion of IL-10 and IL-17 was impaired in the ICOS-deficient patients, in agreement with the previous report (33). To confirm the Th17 defect in the patients, a real-time PCR analysis was used to quantify IL-17A mRNA induction. The results, shown in Fig. 5*C*, demonstrate a significant decrease in relative IL-17A mRNA expression in ICOS-deficient T cells. Furthermore, induction of other cytokines, such as IL-6, IL-12 p40, TNF-α, and TNF-β, in CD4 T cells was impaired to various degrees in the patients (Fig. 5*A*).

Interestingly, the synthesis of the different cytokines was not equally affected in the absence of ICOS: the production of IL-2 was within ±1 SD of normal values, and the IL-22 response was similar to that in controls.

To determine whether the observed defects in effector T cell function can be reproduced by direct activation of intracellular signaling, we examined the capacity of lymphocytes to produce cytokines after PMA/ionomycin stimulation. To that end, intracellular IFN-γ, IL-4, and IL-17 were monitored in PBMCs stimulated with PMA/Ca ionophore by flow cytometry. Fig. 6*A* shows that the CD4 T cells of the patients elicited markedly reduced Th1, Th2, and Th17 cytokine responses.

To corroborate these results, we measured the level of cytokines using a FlowCytomix kit in purified CD4 T cells incubated with PMA and ionomycin for 24 h. A similar trend was noted, as follows: the production of IFN-γ, IL-5, IL-10, TNF-α, and TNF-β was found to be diminished. The capacity of $ICOS^{-/-}$ CD4 T cells to produce IL-2 and IL-6, however, was not markedly impaired (supplemental Fig. 1).[3]

Because $CD45RO^+$ T cells are the major producers of IFN-γ, IL-4, and IL-17 (44) (Fig. 6*A*), we considered the possibility that the impaired cytokine responses were due to the decrease in memory CD4 T cells in the patients. To test this, we stimulated PBMCs with PMA/ionomycin and tested for intracellular IFN-γ, IL-4, or IL-17 in the $CD4^+CD45RO^+$ population. Fig. 6, *A* and *B*, shows that memory T cells of the patients produced less IFN-γ than the controls. In the controls, 30% of $CD45RO^+$ memory T cells produced IFN-γ, whereas in the patients, only ~10% of $CD45RO^+$ memory T cells did so. The synthesis of IL-4 and IL-17 in the memory T cell fraction was marginally decreased in the patients,

[3] The online version of this article contains supplemental material.

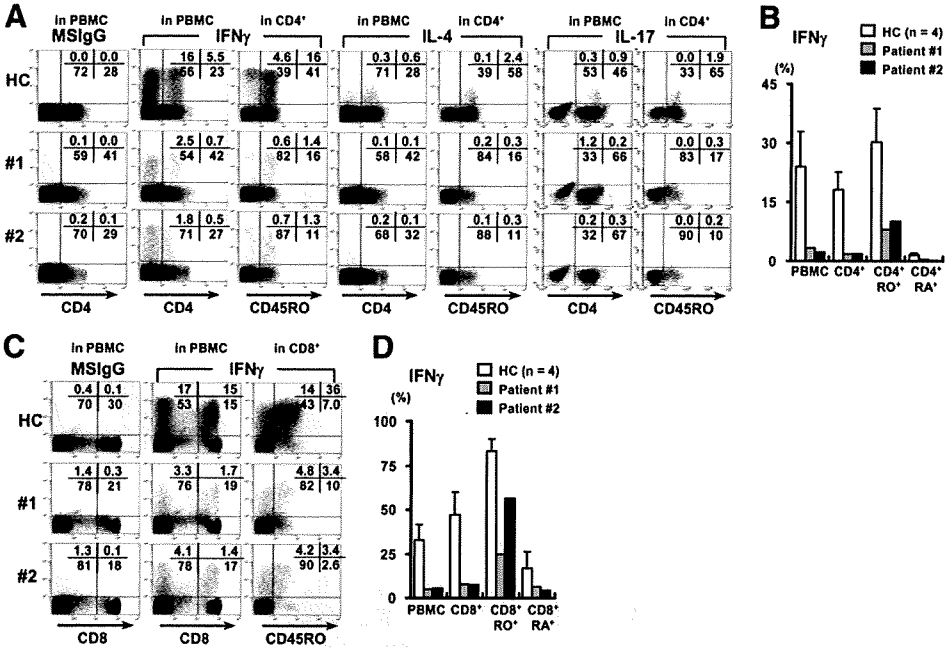

FIGURE 6. Defective cytokine production in T cells stimulated with PMA/ionomycin in ICOS-deficient patients. *A* and *C*, PBMCs were stimulated with PMA and ionomycin for 5 (IL-17) or 8 h (IFN-γ and IL-4). Cells were stained for intracellular IFN-γ, IL-4, and IL-17 together with Abs to CD4 and CD45RO or CD45RA. The same experiment was conducted in CD8 T cells for intracellular detection of IFN-γ. Intracellular staining of each cytokine in CD4 and $CD4^+CD45RO^+$ T cells (*A*) and in CD8 and $CD8^+CD45RO^+$ T cells (*C*) is shown. A representative FACS analysis is illustrated for one of four healthy controls (HC) (for CD4), one of five HC (for CD8), and the patients. *B* and *D*, Pooled data on IFN-γ-producing cells among PBMCs, CD4 T cells, $CD4^+CD45RO^+$ cells, $CD4^+CD45RA^+$ cells, CD8 T cells, and $CD8^+CD45RO^+$ cells, in HC ($n = 4$) and patients 1 and 2. □, HC; ▨, patient 1; ■, patient 2. Error bar for HC indicates SD. The mean percentage obtained from two separate analyses is shown for the patients.

and the decline was not as clear as that observed in IFN-γ production (Fig. 6*A*).

Importantly, the inability to produce IFN-γ does not seem to be restricted to CD4 T cells, because a marked reduction in the IFN-γ response was also evident in the CD4-negative population. To assess effector function of CD8 T cells, we directly measured intracellular IFN-γ in CD8 T cells and a $CD8^+CD45RO^+$ population upon stimulation with PMA/ionomycin. The results displayed in Fig. 6, *C* and *D*, revealed impaired IFN-γ production from CD8 T cells and memory CD8 T cells from the patients. The production of IFN-γ was also significantly reduced in CD8 T cells stimulated through CD3 and CD28 in the patients (Fig. 5*B*).

Mechanism of defective cytokine production in patients: reduced induction of master regulators of Th1, Th2, and Th17 lineage commitment

We next investigated the mechanisms underlying the T cell unresponsiveness in the patients. One potential explanation is that their T cells did not proliferate well or were prone to apoptosis, or both, in the absence of ICOS expression. To examine this possibility, the proportion of cells that underwent PMA/ionophore-induced cell death was assessed by annexin V/7-AAD staining. The results showed that in the patients, this proportion was similar to or rather lower than that in controls. The proliferative capacity of $ICOS^{-/-}$ T cells, as assessed by CFSE staining, showed that their T cells proliferated normally or even more vigorously in response to CD3/CD28 cosignal, with significantly more cells with multiple divisions, relative to controls (supplemental Fig. 2).[3]

Although less likely, the absence of the ICOS-ICOS-L interaction during CD3/CD28 costimulation of CD4 T cells may have contributed to impaired cytokine production in the patients. To test the possible contribution of the ICOS signal in cytokine production, we stimulated purified CD4 T cells from healthy controls ($n = 5$) through CD3/CD28 with or without anti-ICOS-L blocking Ab (45), and measured the level of cytokines in the supernatants. Supplemental Fig. 3, *A–C*,[3] shows that the effect of ICOS blocking is negligible in this cytokine production assay.

Another explanation for the defective production of effector cytokines is that there were fundamental flaws in their development into effector T cell subsets. We therefore investigated the expression of master transcription regulators of Th1, Th2, and Th17 lineage commitments by quantitative real-time PCR.

Purified CD4 T cells were stimulated with PMA/ionomycin for 4 h or anti-CD3/CD28 for 24 h, and the mRNA expression level of T-bet (for the Th1 lineage) (46), GATA3 and MAF (for the Th2 lineage) (47, 48), and RORC/ROR-γt (for the Th17 lineage) (49) was quantified using GAPDH expression as a control, and expressed as relative expression (RE) adjusted for the baseline expression level of healthy controls ($n = 4$), taken as 1.0. We observed reduced PMA/ionophore-driven T-bet induction in $ICOS^{-/-}$ CD4 T cells in the patients, and defective induction was more pronounced in patient 2 (Fig. 7*A*). Compared with controls (RE, 16.2 ± 5.3), CD3/CD28-induced T-bet expression was decreased in patient 1 (RE, 7.2), whereas the reduction was less marked in patient 2 (RE, 12.4) (Fig. 7*B*).

GATA-3 induction was detectable after PMA/ionophore stimulation. In the patients, induction of GATA-3 above the baseline level was virtually absent in CD4 T cells (RE, 1.3 for patient 1, and 1.0 for patient 2) (Fig. 7*A*). The RE values of MAF in CD4 T cells in response to PMA/ionomycin and TCR/CD28 in controls were 3.3 ± 1.4 and 4.4 ± 1.0, respectively. In contrast, stimulation-induced MAF expression was virtually absent in both patients (Fig. 7, *A* and *B*).

We also observed that the expression levels of RORC in ICOS-deficient CD4 T cells stimulated with CD3/CD28 or PMA/ionomycin were diminished more than 2-fold (Fig. 7, *A* and *B*).